Geosci. Model Dev. Discuss., https://doi.org/10.5194/gmd-2018-109
Manuscript under review for journal Geosci. Model Dev.
Discussion started: 2 May 2018

Geoscientific Model Development Discussions

Ecological ReGional Ocean Model with vertically resolved sediments (ERGOM SED 1.0): Coupling benthic and pelagic biogeochemistry of the south-western Baltic Sea

Hagen Radtke[1], Marko Lipka[2], Dennis Bunke[3,4], Claudia Morys[5,6], Bronwyn Cahill[1,7], Michael E. Böttcher[2], Stefan Forster[5], Thomas Leipe[8], and Thomas Neumann[1]

[1]Leibniz Institute for Baltic Sea Research Warnemuende (IOW), Department of Physical Oceanography and Instrumentation, Seestr. 15, 18119 Warnemünde, Germany
[2]Leibniz Institute for Baltic Sea Research Warnemuende (IOW), Department of Marine Geology, Geochemistry and Isotope Biogeochemistry Group, Seestr. 15, 18119 Warnemünde, Germany
[3]Leibniz Institute for Baltic Sea Research Warnemuende (IOW), Department of Marine Geology, Paleooceanography and Sedimentology Group, Seestr. 15, 18119 Warnemünde, Germany
[4]Current address: Leipzig University, Institute of Geophysics and Geology, Talstr. 15, 04013 Leipzig, Germany
[5]University of Rostock, Institute for Biosciences, Albert-Einstein-Str. 3, 18059 Rostock, Germany
[6]Current address: Royal Netherlands Institute for Sea Research (NIOZ), Department of Estuarine and Delta Systems, and Utrecht University, Korringaweg 7, 4401 NT Yerseke, The Netherlands
[7]Current address: Freie Universität Berlin, Institute for Space Science, Carl-Heinrich-Becker-Weg 6-10, 12165 Berlin, Germany
[8]Leibniz Institute for Baltic Sea Research Warnemuende (IOW), Department of Marine Geology, Microanalysis Group, Seestr. 15, 18119 Warnemünde, Germany

Correspondence to: Hagen Radtke (hagen.radtke@io-warnemuende.de)

Abstract. Sediments play an important role in organic matter mineralisation and nutrient recycling, especially in shallow marine systems. Marine ecosystem models, however, often only include a coarse representation of processes beneath the sea floor. While these parametrisations may give a reasonable description of the present ecosystem state, they lack predictive capacity for possible future changes, which can only be obtained from mechanistic modelling.

This paper describes an integrated benthic-pelagic ecosystem model developed for the German Exclusive Economic Zone (EEZ) in the Western Baltic Sea. The model is a hybrid of two existing models: the pelagic part of the marine ecosystem model ERGOM and an early diagenetic model by Reed et al., 2011. The latter one was extended to include the carbon cycle, a determination of precipitation and dissolution reactions which accounts for salinity differences, an explicit description of adsorption of clay minerals and an alternative pyrite formation pathway. We present a one-dimensional application of the model to seven sites with different sediment types. The model was calibrated with observed pore water profiles and validated with results of sediment composition and bioturbation rates collected within the framework of the SECOS project.

Geosci. Model Dev. Discuss., https://doi.org/10.5194/gmd-2018-109
Manuscript under review for journal Geosci. Model Dev.
Discussion started: 2 May 2018

Geoscientific Model Development Discussions

1 Introduction

1.1 Combining models of sedimentary and pelagic biogeochemistry

Marine biogeochemical models and process-resolving sediment models are very similar to each other in terms of their approach. They both try to describe a complex biogeochemical system with a limited set of state variables. Transformation processes are formulated as a set of differential equations, e.g. (van Cappellen and Wang, 1996). These have to obey the principle of mass conservation for any chemical element whose cycle is part of the model system. But in spite of these similarities, and even though both types of models have been extensively applied at least since the 1990s, there have not been many attempts, at least published ones, to combine them into one single benthic-pelagic model system. The review of Paraska et al. (2014), which compares existing sediment model studies, lists 83 publications of which 10 included a coupling to the water column.

A recent attempt to combine sediment and water column biogeochemistry in one model is the study by Yakushev et al. (2017), who developed one of the most complex early diagenetic models published so far and integrated it into the Framework for Aquatic Biogeochemical Models (FABM, www.fabm.net). The FABM generic interface allows coupling to any biogeochemical model within its framework. We would like to refer to their study for a good overview of existing models which bring together water column biogeochemistry with a sophisticated sediment modelling approach. They range from one-dimensional, sediment-centered approaches with a small pelagic extension, e.g. (Reed et al., 2011), to full three-dimensional pelagic ecosystem models which have a complex representation of sedimentary processes and nutrient pools included, e.g. ERSEM (Butenschön et al., 2016). Another recent example is a Black Sea study by Capet et al. (2016), in which the authors applied a hybrid approach with a vertically integrated early diagenetic model. To obtain the partitioning between different oxidation pathways, which is typically determined by the vertical zonation, they ran a one-dimensional, vertically resolved model (OMEXDIA, (Soetaert et al., 1996a)) over a range of different boundary values and fit a statistical meta-model through its output.

To our best knowledge, the first fully coupled benthic-pelagic model system with vertically resolved benthic processes was published by Soetaert et al. (2001). They presented a modelling approach where the biogeochemistry of the Goban Spur shelf ecosystem (North-East Atlantic) was described in a horizontally integrated model. In the present communication we present a similar aproach, adapted to understand the role of the sediments for the ecosystem of the south-western Baltic Sea. The presented one-dimensonal aproach can be seen as an intermediate step towards a fully coupled three-dimensional ecosystem model, with a vertically resolved sediment model coupled under each grid cell. The way to go from the current model to the 3-d version is already pointed out in the model description.

1.2 The German part of the Baltic Sea and the SECOS project

The Baltic Sea is a marginal sea with only narrow and shallow connections to the adjacent North Sea. The small cross sections of these channels, the Danish Straits, and the correspondingly constrained water exchange have several implications for the Baltic Sea system, including the following:

- It is an essentially non-tidal sea.

Geosci. Model Dev. Discuss., https://doi.org/10.5194/gmd-2018-109
Manuscript under review for journal Geosci. Model Dev.
Discussion started: 2 May 2018

- It is brackish due to a mixing between episodically inflowing North Sea water with Baltic river waters which cause an overall positive freshwater balance.
- It shows a pronounced haline stratification.
- It is prone to eutrophication due to the accumulation of mostly river-derived nutrients.

The German Exclusive Economic Zone (EEZ) in the Baltic Sea is situated south of the Danish Straits. It consists of different bights, islands and peninsulas and exhibits a strong zonal gradient and a strong temporal variability in salinity. This varies from 12 to over 20 g kg^{-1} north of the Fehmarn island to 7 to 9 g kg^{-1} in the Arkona Sea (IOW, 2017). In river-influenced near-coastal areas, even lower salinities occur.

Most of the sediment area is characterised by erosion or transport bottoms which only intermittently store deposited material before it is transported further into the central basins of the Baltic Sea (Emeis et al., 2002). Still, during this storage period, organic material is already partly mineralised and inorganic nitrogen is partly removed from the ecosystem by denitrification processes (Deutsch et al., 2010). This transformation of a eutrophic substance into a non-reactive form and its subsequent removal is one example of the type of ecosystem services that coastal sediments can perform.

Understanding and quantifying the scope and scale of such sedimentary services in the German Baltic Sea has been the aim of the SECOS project (2013 - 2019). The project contained a strong empirical part, including several interdisciplinary research cruises focused on the sediments. Seven study sites were selected, based on different granulometric parameters representative of a larger area. These were sampled several times in order to capture the effect of seasonality (see Figure 1). The sampled stations include three sandy sites: Stoltera (ST), Darss Sill (DS) and Oder Bank (OB), a silty site: Tromper Wiek (TW), and three mud sites: Lübeck Bight (LB), Mecklenburg Bight (MB) and Arkona Basin (AB). The TW site has both an intermediate grain size and an intermediate organic matter content, compared to the sandy and muddy sites. In this work, we focus on the development of our coupled one-dimensional benthic-pelagic model system for the German Baltic Sea. We use empirical data obtained from repeated sampling of the SECOS stations to calibrate and validate our early diagenetic model. Further work, discussing the fully coupled three dimensional application of the model to assessing sedimentary services in the German Baltic Sea will be described in a forthcoming paper.

1.3 Article structure

The rest of this paper is structured as follows. Section 2 presents a description of the model and the processes which are included. In Section 3, we summarise which empirical data were used and give a brief explanation on how they were obtained. In Section 4, we describe how these data were used to fit the model to the different stations, since the seven stations mentioned before serve as the test case for our model. The model results are shown and discussed in Section 5. The paper ends in Section 6 with conclusions and an outlook which especially points at the future application of the model in three-dimensional ecosystem models.

Geosci. Model Dev. Discuss., https://doi.org/10.5194/gmd-2018-109
Manuscript under review for journal Geosci. Model Dev.
Discussion started: 2 May 2018

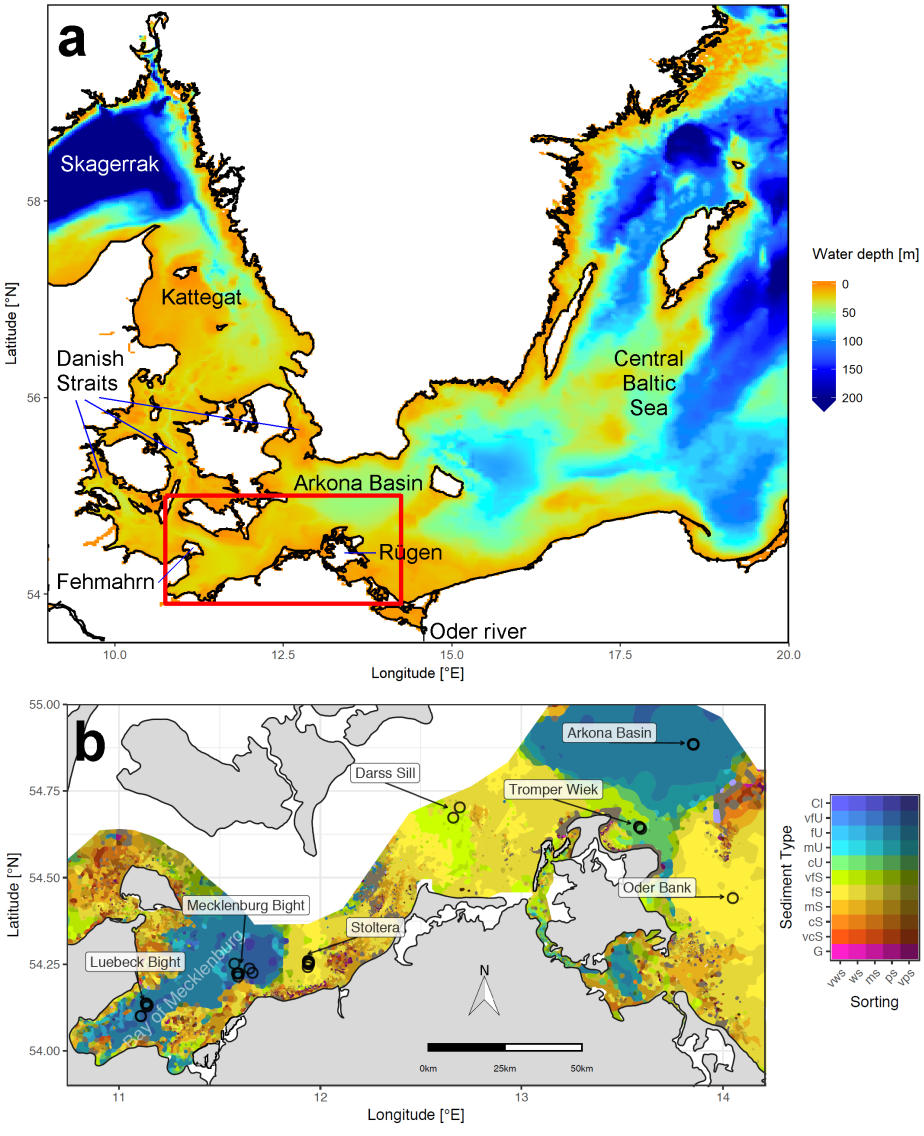

Figure 1. (a) Bathymetry of the Western Baltic Sea and location of our area of interest. (b) The investigation area of the SECOS project. The map shows granulometry, redrawn from Tauber (2012) and Lipka and Böttcher (in prep.), and the seven stations considered in this model study. Sediment Type: Cl = clay, vfU = very fine silt, fU = fine silt, mU = medium silt, cU = coarse silt, vfS = very fine sand, fS = fine sand, mS = medium sand, cS = coarse sand, vcS = very coarse sand, G = gravel; Sorting: vws = very well sorted, ws = well sorted, ms = moderately sorted, ps = poorly sorted, vps = very poorly sorted.

Geosci. Model Dev. Discuss., https://doi.org/10.5194/gmd-2018-109
Manuscript under review for journal Geosci. Model Dev.
Discussion started: 2 May 2018

2 Model description

2.1 Ancestor models

The model is based on two ancestors.

- The water column part is based on ERGOM, an ecological model developed originally for the Baltic Sea (Neumann, 2000). It has been continuously developed since its first publication, the latest improvements introducing refractory dissolved organic nitrogen (Neumann et al., 2015), and transparent exopolymers. It should be mentioned that the light absorption scheme described in Neumann et al. (2015) is not part of the model described here, since they were both developed simultaneously.

  Since the beginning, ERGOM contained three functional groups of phytoplankton, representing large-cell (diatom) and small-cell (flagellate) primary producers as well as diazotroph cyanobacteria, and the ability to simulate hypoxic/anoxic conditions.

- The sediment part is based on a model developed for a study on the effect of seasonal hypoxia on sedimentary phosphorus accumulation in the Arkona Sea (Reed et al., 2011). This model is, as many others of its kind, a descendant of the van Cappellen and Wang (1996) model. This paper focused on the sedimentary iron and manganese cycle, but also contained the mineralisation pathways of oxic mineralisation, denitrification, and sulphate reduction. An extensive literature survey (combined with model fitting to observations) allowed the estimation of a large quantity of model constants such as solubility products and half-saturation constants. These were later on inherited by several early diagenetic models, including the one presented in this article.

2.2 Model compartments and state variables

The one-dimensional model consists of four compartments as shown schematically in Figure 2:

1. The water column,
2. a fluff layer deposited on the sediment surface,
3. the sedimented solids, and
4. the pore water between them.

The water column and the sediment are vertically resolved, the former in layers of 2 m depth such that their number depends on the water depth of the specific site, the latter in 22 layers increasing in depth from 1 mm at the sediment surface to 2 cm at the bottom of the modelled sediment in 22 cm depth. These specific numbers are not intrinsic to the model but can be changed in the input files[1]. The current choice of 22 cm for the sediment depth was taken according to the availability of pore water data.

[1] `physics/cellheights.txt, physics/sed_cellheights.txt`

Geosci. Model Dev. Discuss., https://doi.org/10.5194/gmd-2018-109
Manuscript under review for journal Geosci. Model Dev.
Discussion started: 2 May 2018

Sediment porosity is prescribed[2] and site-specific. As a simplifying assumption, accumulating organic material does not change the porosity. Similarly, the amount of material accumulated in the fluff layer does not change the remaining volume in the bottom water cell.

The tracers (model state variables) present in each of the compartments are listed in Table 1. All of the tracers have a fixed stoichiometric composition which is shown in Appendix A. Where stoichiometric ratios change, such as during detritus decomposition, more than one tracer is needed. This means we can check mass conservation at design time of the model by formulating it in a process-based way as outlined in Radtke and Burchard (2015). To check this mass conservation, the chemical reaction equations need to be formulated in a complete way, which is why "virtual tracers" such as water may be included in the process formulation, even if they do not occur as state variables in the model.

Total alkalinity is a "combined tracer", which means that its rate of change depends on its constituents which are actively produced or consumed. The tracer value changes by 1 unit if (see Table 1)

- `ohminus` is changed by 1 unit or
- `h3oplus` is changed by -1 unit or
- `t_po4` is changed by 0.5 units.

The reasoning behind this is explained in Section 2.6.

The state variables will not be discussed one-by-one here, but rather in the section about the biogeochemical processes (Sections 2.4 and 2.5), where their role in the ecosystem will be explained.

Virtual tracers do not occur as a state variable in the model, but only as balancing terms in the biogeochemical process equations. They make it easier to check that the mass balance of all chemical elements is maintained.

2.3 Transport processes

The processes which transport the tracers vertically are schematically shown in Figure 2. Their detailed implementation is discussed here.

Horizontal exchange (transport) is neglected in our one-dimensional model. This is obviously an inadequate approximation for the water column processes, as we do not consider basins, but rather single stations, some of which are situated in proximity to river mouths, where lateral transport processes have a major impact. We solve this issue in the future application of the biogeochemical model in a three-dimensional model system (Cahill et al., in prep.).

In this model, we are not specifically interested in the water column as such but rather see it as being responsible for delivering the right amount of sedimenting detritus at the right time. To obtain this, we relax the wintertime nutrients in the surface layer to a realistic value. This may be seen as a parameterisation of a lateral exchange process. In addition, transport of fluff layer material away from or towards the modelled location is a lateral process included in the model.

[2] `physics/sed_inert_ratio.txt`

Geosci. Model Dev. Discuss., https://doi.org/10.5194/gmd-2018-109
Manuscript under review for journal Geosci. Model Dev.
Discussion started: 2 May 2018

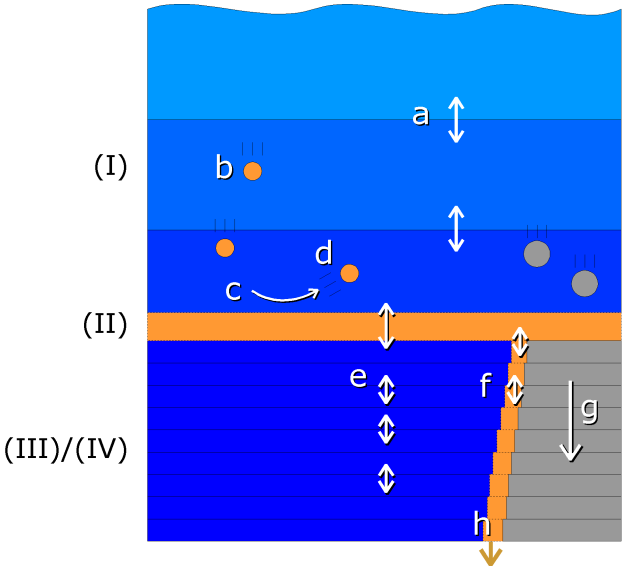

Figure 2. Schematic view of the compartments and vertical exchange processes in the model. Compartments: (I) water column, (II) fluff layer, (III) pore water, (IV) solid sediment. Both water column and sediment consist of several vertically stacked grid cells. Vertical transport processes: a = turbulent mixing, b = particle sinking, c = sedimentation, d = resuspension, e = bioirrigation combined with molecular diffusion, f = bioturbation, g = sediment growth, h = burial. Bioactive solid material is shown in orange, bioinert solid material in grey and water in blue.

The parametrisations of these lateral transport processes are not discussed in this section, but together with the biogeochemical processes to which they closely correspond in Section 2.4. All other physical processes included will be described here, but only in a qualitative way. For a quantitative description including the model constants we refer to the online supplementary material.

2.3.1 Turbulent mixing

The vertical exchange due to turbulent mixing in the water column is prescribed externally[3] by a turbulent diffusivity. In our case, it is taken from a three-dimensional MOM5 model run (Radtke, unpublished). In this model setup, turbulent vertical mixing is estimated by the KPP turbulence parameterisation (Large et al., 1994), which considers both local mixing and, in case of unstable stratification, (non-local) convection. We only take into account the local part of the mixing and apply it to all tracers in the water column.

[3] `physics/diffusivity.txt`

Geosci. Model Dev. Discuss., https://doi.org/10.5194/gmd-2018-109
Manuscript under review for journal Geosci. Model Dev.
Discussion started: 2 May 2018

Geoscientific Model Development Discussions
Open Access
EGU

Table 1. Tracers used in the ERGOM v1.2sed model

name	W	F	S	P	description	unit
t_lpp	+				large-cell phytoplankton	mol kg^{-1} (N units)
t_spp	+				small-cell phytoplankton	mol kg^{-1} (N units)
t_cya	+				diazotroph cyanobacteria	mol kg^{-1} (N units)
t_zoo	+				zooplankton	mol kg^{-1} (N units)
t_det_?	+				detritus, N+C, fast decaying (1) to inert (6)	mol kg^{-1} (N units)
t_detp_?	+				phosphate in detritus, fractions 1 to 6	mol kg^{-1} (N units)
t_don	+				autochthonous dissolved organic nitrogen	mol kg^{-1}
t_poc	+				particulate organic carbon	mol kg^{-1}
t_ihw	+				suspended iron hydroxide	mol kg^{-1}
t_ipw	+				suspended phosphate bound to iron-III	mol kg^{-1}
t_mow	+				suspended manganese oxide	mol kg^{-1}
t_n2	+			+	dissolved molecular nitrogen	mol kg^{-1}
t_o2	+			+	dissolved molecular oxygen	mol kg^{-1}
t_dic	+			+	dissolved inorganic carbon	mol kg^{-1}
t_alk	+			+	total alkalinity	mol kg^{-1}
t_nh4	+			+	ammonium	mol kg^{-1}
t_no3	+			+	nitrate	mol kg^{-1}
t_po4	+			+	phosphate	mol kg^{-1}
t_h2s	+			+	hydrogen sulphide	mol kg^{-1}
t_sul	+			+	elemental sulphur	mol kg^{-1}
t_so4	+			+	sulphate	mol kg^{-1}
t_fe2	+			+	ferrous iron	mol kg^{-1}
t_ca2	+			+	dissolved calcium	mol kg^{-1}
t_mn2	+			+	dissolved manganese-II	mol kg^{-1}
t_sil	+			+	silicate	mol kg^{-1}
t_ohm_quickdiff	+			+	OH- ions with realistically quick diffusion	mol kg^{-1}
t_ohm_slowdiff	+			+	OH- ions which move unrealistically slow with alkalinity	mol kg^{-1}
t_sed_?		+	+		sedimentary detritus N+C, fractions 1 to 6	mol m^{-2} (N units)
t_sedp_?		+	+		phosphate in sedimentary detritus, fractions 1 to 6	mol m^{-2} (N units)
t_ihs		+	+		iron hydroxide in the sediment	mol m^{-2}
t_ihc		+	+		iron hydroxide in the sediment - crystalline phase	mol m^{-2}
t_ips		+	+		iron-bound phosphate in the sediment	mol m^{-2}
t_ims		+	+		iron monosulphide	mol m^{-2}
t_pyr		+	+		pyrite	mol m^{-2}
t_mos		+	+		manganese oxide in the sediments	mol m^{-2}
t_rho		+	+		rhodochrosite	mol m^{-2}
t_i3i		+	+		potentially reducible iron-III in illite-montmorillonite mixed layer minerals	mol m^{-2}
t_iim		+	+		iron-II adsorbed to illite-montmorillonite mixed layer minerals	mol m^{-2}
t_pim		+	+		phosphate adsorbed to illite-montmorillonite mixed layer minerals	mol m^{-2}
t_aim		+	+		ammonium adsorbed to illite-montmorillonite mixed layer minerals	mol m^{-2}
h2o		virtual			water molecule	
h3oplus		virtual			hydronium ion	
ohminus		virtual			hydroxide ion	
i2i		virtual			structural iron-II in illite-montmorillonite mixed-layer minerals	

W: Water column, F: Fluff layer, S: Solid sediment, P: Pore water

Geosci. Model Dev. Discuss., https://doi.org/10.5194/gmd-2018-109
Manuscript under review for journal Geosci. Model Dev.
Discussion started: 2 May 2018

2.3.2 Particle sinking

In our model, suspended particulate matter sinks at a constant rate through the water column. We choose 4.5 m day^{-1} for detritus, 1 m day^{-1} for manganese and iron oxides, including the phosphate adsorbed by them, and 0.5 m day^{-1} for large-cell phytoplankton and particulate organic carbon. In contrast, cyanobacteria are not sinking but, due to their positive buoyancy, they show an upward movement of 0.1 m day^{-1}. In reality, the sinking rate differs between individual particles; the currently chosen average values are a result of fitting the previous ERGOM model with the simplified sediment representation to observations.

2.3.3 Sedimentation and resuspension

The shear stress at the bottom determines whether erosion or sedimentation takes place. We apply the combined shear stress of currents and waves calculated by the same MOM5 model as the turbulent mixing. If this shear stress is below a critical value of 0.016 N m^{-2} (Christiansen et al., 2002), the sinking suspended matter accumulates in the fluff layer compartment. If it is exceeded, the fluff layer material is resuspended into the lowest water cell at a constant relative rate.

In our model, no material will ever be resuspended from the sediment itself, which starts below the fluff layer. This means that our model is incapable of realistically capturing extreme events like storms or bottom trawling which winnow the upper layers of the sediment, removing the organic material which has a lower sinking velocity from the heavier mineral components (Bale and Morris, 1998). It also neglects a washout, that is, the removal of organic matter from the sediment pores by advective transport of pore water by strong bottom currents (Rusch et al., 2001). In our model, sediment reworking by currents and waves is not explicitly represented, but rather parametrised together with the bioturbation process. This process allows a bi-directional exchange of particulate material between sediment and fluff layer, see Section 2.3.5. The upward component of the transport represents winnowing of sediments (Bale and Morris, 1998).

2.3.4 Bioerosion

In environments with oxic bottom waters, we assume that in addition to waves and currents, macrofaunal animals or demersal fish can resuspend organic material from the fluff layer by active movements. Therefore, under oxic conditions, we assume that 3 % day^{-1} of the fluff material is resuspended independently from the shear stress conditions.

2.3.5 Bioturbation

Bioturbation describes the movement and mixing of particles inside the sediment caused by animals.[4] In fact, it is hard to discriminate what causes the vertical mixing of particles; also physical effects like bottom shear may have the same effect. We therefore include them in our "bioturbation" process.

[4]While bioturbation in reality causes both a transport of solids and solutes, we use the term "bioturbation" in the model to describe the transport of solids only, while the transport of solutes is done by the "bioirrigation" process.

Geosci. Model Dev. Discuss., https://doi.org/10.5194/gmd-2018-109
Manuscript under review for journal Geosci. Model Dev.
Discussion started: 2 May 2018

Geoscientific Model Development Discussions

We consider bioturbation to act as a vertical diffusivity on the concentrations of the different solid species in the sediment. This implies we exclude non-local mixing processes, even if they may be important in nature (Soetaert et al., 1996b), and try to represent them by local mixing.

The vertical mixing follows the equation

$$\frac{\partial}{\partial t}(1-\phi)c \quad = \quad \frac{\partial}{\partial z}\left((1-\phi)D_{B,solids}\frac{\partial c}{\partial z}\right), \tag{1}$$

(Boudreau, 1997). Here $c(z,t)$ denotes a tracer concentration with respect to the volume of the solids only, $D_{B,solids}(z)$ is the bioturbation intensity and $\phi(z)$ is the porosity. This equation only takes intraphase mixing into account, which means we assume that the porosity remains constant over time. The factor $(1-\phi)$ relates the concentration to the total (solid + liquid) volume of the sediment.

The same equation is also applied to describe the transport between the uppermost sediment layer and the fluff, which is caused by benthic organisms. In reality, the fluff layer may strongly differ in its compaction (porosity) depending on the turbulence conditions. We, however, assume it to be perfectly compacted ($\phi = 0$) to be able to apply the above equation to describe the exchange process, and therefore assume a thickness of 3 mm. This is not a physical assumption but rather a numerical trick which we use to transport the fluff material into the sediments. In reality, this incorporation of organic matter is done by macrofaunal activities, e.g. (van de Bund et al., 2001).

The vertical structure of bioturbation intensity, $D_{B,solids}(z)$, is parametrised vertically as follows: In the uppermost part of the sediment, we assume a constant bioturbation rate. Below that, it decays exponentially with depth until it reaches a maximum depth, which may be below the bottom of our model. So we externally prescribe (a) the maximum mixing intensity[5] and (b) three length scales describing the vertical structure of bioturbation[6], which are the depth down to which the maximum mixing rate is applied, the length scale of exponential decay of the mixing rate below this depth, and the maximum depth of mixing.

2.3.6 Bioirrigation

Bioirrigation describes the mixing of solutes within the pore water and the exchange with the bottom water. To model it, we apply a similar equation,

$$\frac{\partial}{\partial t}\phi c \quad = \quad \frac{\partial}{\partial z}\left(\phi D_{B,liquids}\frac{\partial c}{\partial z}\right), \tag{2}$$

(Boudreau, 1997). Here $c(z,t)$ denotes a tracer concentration with respect to the volume of the pore water only and $D_{B,liquids}(z)$ is the bioirrigation intensity. Again we assume that the porosity is constant in time. We also use this equation for the solute exchange between the pore water and the overlying bottom water cell. The vertical profile of bioirrigation intensity is assumed identical to that of bioturbation. The maximum bioirrigation rate is assumed constant in time and prescribed externally[7].

[5] `physics/sed_diffusivity_solids.txt`
[6] `physics/sed_depth_bioturbation.txt`
[7] `physics/sed_diffusivity_porewater.txt`

Geosci. Model Dev. Discuss., https://doi.org/10.5194/gmd-2018-109
Manuscript under review for journal Geosci. Model Dev.
Discussion started: 2 May 2018

2.3.7 Molecular diffusion

Molecular diffusion in the sediment is described by the equation

$$\frac{\partial}{\partial t}\phi c = D_0 \frac{\partial}{\partial z}\left(\frac{\phi}{\theta^2}\frac{\partial c}{\partial z}\right), \quad (3)$$

(Boudreau, 1997). Here D_0 describes the molecular diffusivity in a particle-free solution, which is effectively reduced by the effect of hydrodynamic tortuosity θ. This describes the effect that the solutes need to travel a longer path as the direct way may be obstructed by solid particles. It is estimated from porosity by $\theta^2 = 1 - 2.02\ln(\phi)$ (Boudreau, 1997).

A diffusive exchange between the pore water and the overlying bottom water is controlled by the thickness of a diffusive boundary layer. While in reality this relates to the viscous sublayer thickness and is therefore inversely related to the velocity of the bottom water (Boudreau, 1997), we for simplicity assume a constant diffusive boundary layer thickness of 3 mm.

Molecular diffusivities for the different solute species are calculated from water viscosity following Boudreau (1997). The water viscosity is determined from salinity and temperature (assumed to be identical to that in the bottom water cell).

A problem occurs with the combined tracers DIC and total alkalinity, as they do not represent a specific ion but rather a set of different species with different molecular diffusivities. For simplicity, we approximate DIC diffusivity to be that of the HCO_3^- ion, the most common one at the pH values we expect. For total alkalinity, we take a two-step approach: In the first step, we also take the diffusivity of the HCO_3^- ion. But this is an underestimate especially for the OH^- ions which increase in their concentration as the solution becomes alkaline. To take their higher diffusivity into account, we introduce two additional tracers, `t_ohm_slowdiff` and `t_ohm_quickdiff`. Before the molecular diffusion is applied during a model time step, they are both set equal to the OH^- concentrations. During the diffusion time step, the former diffuses with the reduced HCO_3^- diffusion rate, the latter with the OH^- diffusivity. So afterwards, total alkalinity is corrected by adding the difference of the two, `t_ohm_quickdiff-t_ohm_slowdiff`. This results in a smoothed alkalinity profile.

2.3.8 Sediment accumulation

In nature, sediments grow upwards as new particulate matter sediments onto them. In our model, this process is taken into account, but represented as a downward movement of material in the sediment. So our coordinate system moves upward with the sediment surface.

We assume that the sediment growth is supplied by terrigenous, bioinert material, and prescribe[8] a growth rate from literature for the mud stations only, (Table 2). For the sand and silt stations we do not assume sediment growth.

We use a simple Euler-Forward advection to move the material from each grid cell into the cell below. Material leaving the model through the lower boundary is lost. Only for organic carbon, we assume that a part of it is mineralised, as will be explained in Section 2.5.1. In the top cell, new organic material from the fluff layer enters by sediment growth.

[8] `physics/sed_inert_deposition.txt`

Geosci. Model Dev. Discuss., https://doi.org/10.5194/gmd-2018-109
Manuscript under review for journal Geosci. Model Dev.
Discussion started: 2 May 2018

2.3.9 Parameterisation of lateral transport

The Baltic Sea sediments can be classified as accumulation, transport and erosion bottoms (Jonsson et al., 1990). The lateral transport of matter is characterised by movement from the transport and erosion bottoms in the shallower areas to the accumulation bottoms in the deep basins (Christiansen et al., 2002). As this process is not represented in our 1-d model setups, we need to parametrise it.

For the sandy and silty sediments, we assume a transport away from the site. This is described by a constant removal rate for all material deposited in the fluff layer.

For the mud stations, we assume a transport of organic material towards the site. This is described by a constant input of detritus. Our model contains six detritus classes which degrade at different rates, as will be explained later, in Section 2.4.4. We assume that the quickest-degradable part of the detritus is already mineralised during the lateral migration and therefore exclude the first two classes from this artificial input.

In the 3-d version of the model, these processes are no longer required, as the material removed from the shallow sites is transported to the deeper ones.

2.4 Biogeochemical processes in the water column

In this section, we describe the biogeochemical processes acting in the water column. These are mostly identical to previously published ERGOM versions, which contained a more simple, vertically integrated sediment model. As in the previous section, we provide the quantitative description including the model constants in the online supplement.

2.4.1 Primary production and phytoplankton growth

There are three classes of phytoplankton in the model, representing large-cell and small-cell microalgae as well as diazotroph cyanobacteria. Their growth is determined by a class-specific maximum growth rate, but contains two limiting factors, for nutrients and light. The light limitation is a saturation function with optimal growth at a class-specific optimum level or at 50% of the surface radiation. The short wave light flux at the surface is taken from a dynamically down-scaled ERA40 atmospheric forcing (Uppala et al., 2005), using the regional Rossby Centre Atmosphere model (RCA). Nutrient limitation is a quadratic Michaelis-Menten term for DIN (nitrate + ammonium) or phosphate, depending on which one is limiting, based on Redfield stoichiometry. Diazotroph cyanobacteria are only limited by phosphate and not by DIN, but they are only allowed to grow in a specific salinity range. Cyanobacteria and small-cell algae also require a minimum temperature to grow (Wasmund, 1997; Andersson et al., 1994).

In case that nutrients are limiting, photosynthesis continues at the same rate and consumes DIC, producing dissolved oxygen. Carbon is then exudated in the form of transparent exopolymers (Engel, 2002), which are assumed to have a constant sinking velocity.

Geosci. Model Dev. Discuss., https://doi.org/10.5194/gmd-2018-109
Manuscript under review for journal Geosci. Model Dev.
Discussion started: 2 May 2018

2.4.2 Phytoplankton respiration and mortality

We assume a constant respiration of phytoplankton which is proportional to its biomass. As the model maintains the Redfield ratio, the respiration goes along with an excretion of ammonium and phosphate. A small fraction of the nitrogen is released as dissolved organic nitrogen (DON). In the model, this represents the DON fraction which is less utilizable by phytoplankton, while the fraction with high bioavailability is considered to be part of the ammonium state variable.

Phytoplankton experiences a constant background mortality. An additional mortality is generated by grazing of zooplankton as described next.

2.4.3 Zooplankton processes

Zooplankton is only represented as one bulk state variable.

It grows by assimilating any type of phytoplankton, however, it has a smaller food preference for the cyanobacteria class compared to the other classes. The uptake becomes limited by a Michaelis-Menten-function if the zooplankton´s food approaches a saturation concentration. Feeding can only take place in oxic waters and is temperature-dependent. It shows a maximum at an optimum temperature and a double-exponential decrease when this temperature is exceeded.

Both zooplankton respiration and mortality represent a closure term for the model. They are meant to include the respiration and mortality of the higher trophic levels (fish) which feed on zooplankton, therefore we use a quadratic closure. Mortality is additionally enhanced under anoxic conditions which, however, do not occur in our study area.

2.4.4 Mineralisation processes

The description of detritus[9] differs from the previous ERGOM versions. We have split the detritus into six classes, depending on its degradability. This degradability is described as a decay rate constant, which ranges from 0.065 day^{-1} for the first class to $1.6 \cdot 10^{-5}$ day^{-1} for the fifth class, while the last one is assumed to be completely bioinert. This type of model is known as a "multi-G model", (Westrich and Berner, 1984). The mineralisation is, however, temperature dependent by a Q_{10} rule, as it is realised by microbial processes; the values given above are valid at 0°C.

When detritus is created by plankton mortality, it is partitioned into the different classes in a constant ratio. This ratio was determined from a fit of the multi-G model to an empirical relation between detritus age and its relative decay rate which was proposed by Middelburg (1989). The fraction of non-decaying detritus was estimated from empirically determined carbon burial rates in the Baltic Sea (Leipe et al., 2011).

The chemical composition of detritus is, in contrast to phyto- and zooplankton, not determined by the Redfield ratio. It is enriched in carbon and phosphorus by 50 %, such that it has a C:N:P ratio of 159:16:1.5. This resembles detritus compositions as they were determined in sediment traps and by investigating fluffy layer material in the Baltic Sea (Heiskanen and Leppänen, 1995; Emeis et al., 2000, 2002; Struck et al., 2004).

[9]Throughout the manuscript, we use the term "detritus" in its biological meaning. Here it describes dead particulate organic material only, as opposed to its use in geology, where the term includes deposited mineral particles.

Geosci. Model Dev. Discuss., https://doi.org/10.5194/gmd-2018-109
Manuscript under review for journal Geosci. Model Dev.
Discussion started: 2 May 2018

Geoscientific Model Development Discussions

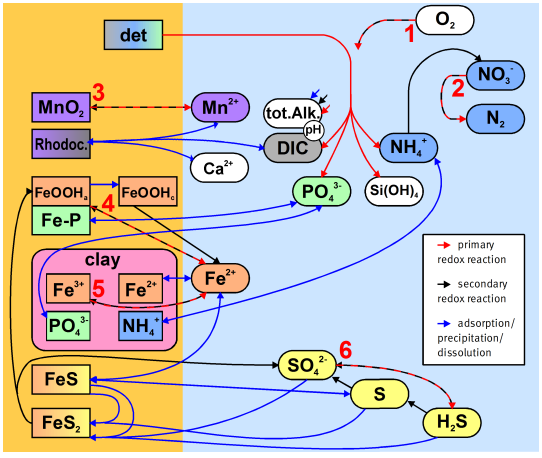

Figure 3. Simplified sketch of state variables and processes in the sediment model. Boxes to the left and right indicate sediment and pore water state variables, respectively. pH is not a state variable but calculated from DIC and total alkalinity. Red arrows show primary redox processes, driven by oxidation of organic carbon. The red numbers indicate the order in which the oxidants are utilised. Black arrows show secondary redox reactions, which means reoxidation of reduced substances. Blue arrows show adsorption/desorption or precipitation/dissolution reactions, which may depend on pH. Abbreviations: det = detritus, Rhodoc. = rhodochrosite, tot.Alk. = total alkalinity, DIC = dissolved inorganic carbon

In the water column, detritus can be mineralised by three different oxidants: oxygen, nitrate and sulphate. They are utilised in this order; if the preferential oxidant's concentration declines, the specific pathway is reduced by a Michaelis-Menten limiter and the next pathway takes over such that the total mineralisation is held constant. In all pathways, DIC, ammonium and phosphate are released. Nitrate reduction also produces molecular nitrogen (heterotrophic denitrification), sulphate reduction generates hydrogen sulphide.

Mineralisation of particulate organic carbon in transparent exopolymers takes place via the same pathways, but only releases DIC. DON is also mineralised after some time and decays to ammonium (which may represent the transformation to bioavailable DON compounds).

2.4.5 Reoxidation of reduced substances

In the presence of oxygen, ammonium is nitrified to nitrate, e.g. (Guisasola et al., 2005). The intermediate step, formation of nitrite, is omitted in the model.

Hydrogen sulphide can be reoxidised by oxygen or by nitrate (chemolithoautotrophic denitrification), e.g. (Bruckner et al., 2013). This takes place as a two-step process via the formation of elemental sulphur (Jørgensen, 2006).

All reoxidation processes exponentially increase their rates with temperature.

Geosci. Model Dev. Discuss., https://doi.org/10.5194/gmd-2018-109
Manuscript under review for journal Geosci. Model Dev.
Discussion started: 2 May 2018

2.5 Biogeochemical processes in the fluff layer, sediment and pore water

In this section, we qualitatively describe the sedimentary biogeochemical processes contained in the model. For a quantitative description including the model constants, we refer to the online supplementary material. Figure 3 gives a schematic overview of the processes considered in the sediment model. As every model, the chosen set of biogeochemical processes and variables does not aim at completeness in its representation of reality, but rather at the strongest possible simplification which still retains the required complexity to describe the processes we are interested in. For this reason, we do not, for example, consider methane formation explicitly.

2.5.1 Mineralisation in general

The mineralisation of detritus is the dominant biogeochemical process in the sediments, as the oxidation of the carbon therein is the major supply of chemical energy for microbes.

As in the water column, oxidants are utilised in a specific order, and a smooth transition to the next mineralisation pathway occurs when the preferred one gets exhausted. However, the number of possible oxidants is increased in the sediment, as here also solid components may act as electron acceptors. The order in which they are utilised is (Boudreau, 1997):

1. oxygen
2. nitrate
3. manganese oxide
4. iron oxyhydroxide
5. iron-III contained in clay minerals
6. sulphate

After sulphate is exhausted, typically the formation of methane would start. This process is omitted in the current model, as we designed our model for the top 22 cm of the German part of the Baltic Sea, where we do not expect sulphate to be limiting. This depth restriction is based on the limited length of the sediment cores taken in the empirical part of our research project. We do, however, describe the process implicitly, since we assume that a part of the organic carbon which leaves the model domain through the lower boundary will be transformed to methane, which, as it diffuses upward will be oxidised by sulphate and generate H_2S. Therefore, we parametrise this process by a conversion from sulphate to hydrogen sulphide at the lower boundary.

As in the water column, we distinguish between six different classes of detritus with different basic mineralisation rates. These rates are only controlled by temperature, not by the specific oxidant which is available. There is an ongoing controversy as to what determines the rate of sedimentary carbon decay, whether it is the oxidant (and therefore the accessible energy per mole of carbon) or the degradability of the detrital carbon itself (Kristensen et al., 1995; Arndt et al., 2013). In leaving

out the explicit dependence of the oxidant, we do not favour the latter theory; we chose to adopt the decay rates proposed by Middelburg (1989), which may implicitly take the effect of the oxidant into account. This can be interpreted as an implicit assumption that this effect will not differ too much between our modelled sites and the ones investigated in their study.

Sedimentary organic phosphorus (OP) may degrade faster than the corresponding nitrate and carbon, an effect known as preferential P mineralisation (Ingall and Jahnke, 1997). We include this by introducing additional state variables `t_detp_n` for each class `n` of detritus, describing the OP concentration, as well as a constant `pref_remin_p` which describes a constant ratio between the mineralisation speeds of OP and organic carbon and nitrogen. This approach follows Reed et al. (2011).

2.5.2 Specific mineralisation processes

Here we describe the implementation of the primary redox reactions, indicated by the red numbers in Figure 3.

Oxic mineralisation and heterotrophic denitrification are formulated in the same way as in the water column, see Section 2.4.4.

The next pathway is the reduction of Mn-IV to Mn-II which produces dissolved manganese.

The reduction of iron oxyhydroxides should produce dissolved iron-II. This, however, may precipitate very quickly, especially where hydrogen sulphide is present. So for numerical reasons, we combine these reactions, and the reduced iron-III is directly converted into iron monosulphide or considered as adsorbed by clay minerals, as we describe below in 2.5.3.

Some clay minerals, especially sheet silicates which are abundant in the German part of the Baltic Sea (Belmans et al., 1993), contain structural iron which is available for redox reactions, e.g. (Jaisi et al., 2007). We prescribe a station-specific content of these minerals and assume that they contain a small amount of reducible iron, because in a particle analysis of sheet silicates from the investigated area (Leipe, unpublished data), we found slightly lower iron contents in the sulfidic zone compared to the surface area.

Sulphate reduction produces hydrogen sulphide. As discussed above, it represents the terminal mineralization process in our model.

2.5.3 Precipitation and dissolution reactions

Solids can precipitate from a solution when it becomes oversaturated. This happens in an aqueous solution when the actual ion activity product exceeds the respective solubility product and a critical degree of supersaturation is reached.

Diagenetic models often simplify the calculation by multiplying the concentrations rather than the activities, e.g. (van Cappellen and Wang, 1996). The resulting product is then proportional to the actual solubility product as long as the ionic strength of the solution does not change. As the ionic strength of sea water is almost completely defined by its salinity (Millero and Leung, 1976), this assumption is well justified for most marine environments. The Baltic Sea, however, is a brackish sea with strong spatial and temporal changes of bottom salinity, especially in the western part, e.g. (Leppäranta and Myrberg, 2009). For this reason, we take the activity coefficients, which transform concentrations to activities, into account. This is done by

Geosci. Model Dev. Discuss., https://doi.org/10.5194/gmd-2018-109
Manuscript under review for journal Geosci. Model Dev.
Discussion started: 2 May 2018

Geoscientific Model Development Discussions

using the Davies equation (Davies, 1938), which determines the activity coefficient a_i as

$$\log_{10}(a_i) = -Az_i^2\left(\frac{\sqrt{I}}{1+\sqrt{I}} - 0.3 \cdot I\right), \quad (4)$$

where I is the ionic strength, z_i is the ion charge, and A is the Davies parameter, calculated from the dielectric constant of water after Stumm and Morgan (2012), Table 3.3, and Gadani et al. (2012).

Ca-Rhodochrosite precipitates at elevated concentrations of manganese and carbonate. Its solubility product is composition dependent, as the Ca:Mn ratio varies (Böttcher, 1997; Böttcher and Dietzel, 2010). For Baltic Sea muds where ratios around 0.6 occur, an effective solubility product (including the effect of oversaturation) of $10^{-9.5}$ to 10^{-9} M^2 can be deduced from (Jakobsen and Postma, 1989). If the solution becomes undersaturated, rhodochrosite will be dissolved again.

Iron monosulphide precipitates on contact of dissolved iron-II and sulphide, depending on pH, with a solubility product taken from Morse et al. (1987). But, as stated in Section 2.5.2, we assume for numerical reasons that this process takes place directly after iron-III reduction. The solubility product is then used in an inverse way to determine the equilibrium concentration of dissolved iron-II at the current pH, sulphide concentration, and salinity. We then assume a precipitation or dissolution of iron monosulphide which relaxes the present concentration of Fe-II against this equilibrium. This is in agreement with a pore water chemistry model for the central Baltic Sea (Kulik et al., 2000), which states that dissolved iron concentrations in the pore water are buffered by iron sulphides (mackinawite and greigite). The dissolution of iron monosulphide also takes place if clay minerals in the same grid cell are capable of adsorbing additional iron-II. This process is described in Section 2.5.5.

As a simplification, we neglect the change in porosity which would be caused by precipitation (or dissolution) of any solids.

2.5.4 Pyrite formation

Pyrite (FeS_2) is a crystalline compound formed in early diagenesis (Rickard and Luther, 2007), its formation from iron monosulphide is included in most early diagenetic models. This process is not a simple precipitation process, but rather a redox process. While both sulphide and iron monosulphide contain sulphur of oxidation state -2, the redox state of S in pyrite is -1. This implies that an electron acceptor is required to create pyrite. A generally accepted mechanism for pyrite creation is the use of zero-valent sulphur from polysulphides, this may be created by oxidation of sulphate with iron-III. However, this process alone cannot explain the high degrees of pyritisation in Baltic deep sediments (Boesen and Postma, 1988).

An additional pathway which does not rely on elemental sulphur, but instead reduces hydrogen sulphide to hydrogen gas, has been proposed by Drobner et al. (1990) and Rickard and Luther (1997). Similar to how it was done in early diagenetic models, e.g. (Wijsman et al., 2002), we include this pathway and therefore assume that whenever iron monosulphide and H_2S are present, pyrite is formed from them. The generated H_2 will be consumed by sulphate-reducing bacteria (Stephenson and Stickland, 1931), so in the net reaction, sulphate acts as the electron acceptor.

Geosci. Model Dev. Discuss., https://doi.org/10.5194/gmd-2018-109
Manuscript under review for journal Geosci. Model Dev.
Discussion started: 2 May 2018

2.5.5 Adsorption balances

Adsorption in our model takes place on the surfaces of two particle types: iron oxyhydroxides and clay minerals. Adsorption on silicate particles is not explicitly represented in the model, but parametrised by a reduction of the effective diffusivity of phosphate and ammonium, following Boudreau (1997).

Iron oxyhydroxides adsorb dissolved phosphate. This is a well-known process responsible for the sedimentary retention of phosphate derived from mineralisation processes, e.g. (Sundby et al., 1992). As both phosphate and hydroxide ions can occupy the adsorption sites at the surface, adsorption is less efficient in alkaline environments.

In our model, we use a formula from Lijklema (1980) which describes the adsorbed P:Fe ratio at a given phosphate concentration and pH. But we use it inversely. We calculate an equilibrium concentration for dissolved phosphate at the current P:Fe ratio and pH. If the current concentration of dissolved phosphate is above this equilibrium concentration, adsorption takes place and PO_4 in the pore water is decreased. If it is below the equilibrium concentration, desorption takes place.

Following Reed et al. (2011), we define two classes of iron oxyhydroxides. The first one is fresh, amorphous and adsorbs phosphate. The second one is a more crystalline phase, for which we assume no adsorption. The first phase is transformed to the second one with a constant rate in time, implying a continuous phosphate release.

Clay minerals, due to their large surface area, can also adsorb pore water species. We allow an adsorption of phosphate, ammonium and iron-II. For simplicity, we assume that the ratio of adsorbed species to clay mass is proportional to the pore water concentration, until a saturation threshold is exceeded. For iron-II, this proportionality constant is derived from Jaisi et al. (2007), for ammonium from Raaphorst and Malschaert (1996), and for phosphate from Edzwald et al. (1976).

In all three cases, we calculate a pore water concentration which is in equilibrium with the current ratio of adsorbed species to clay mineral mass. Then adsorption or release processes take place to relax the present pore water concentration towards the equilibrium value. In the case of iron-II, however, for numerical reasons we allow an immediate precipitation of the desorbed iron-II as iron monosulphide in case of its oversaturation, leaving out the intermediate transformation to dissolved Fe-II. The inverse is also true, if iron monosulphide is dissolved, the released iron-II may directly be adsorbed by the clay minerals instead of being released to the pore water first.

2.5.6 Reoxidation of reduced substances

Ammonium is oxidised to nitrate in the presence of oxygen. The rate of this process is proportional to both the ammonium and the oxygen concentration and, as in the water column, increases exponentially with temperature.

Dissolved manganese-II will be oxidised in the presence of oxygen and precipitates as manganese oxide. This is also assumed to be a second-order process proportional to both precursor concentrations.

Dissolved iron-II is oxidised by oxygen in a pH-dependent way. The rate of this process is proportional to the iron-II and oxygen concentration, as well as to the square of the hydronium ion concentration. It is also influenced by temperature and ionic strength, as described by Millero et al. (1987). For numerical reasons, we also allow a direct oxidation of iron-II adsorbed

Geosci. Model Dev. Discuss., https://doi.org/10.5194/gmd-2018-109
Manuscript under review for journal Geosci. Model Dev.
Discussion started: 2 May 2018

to clay minerals. Alternatively, dissolved iron-II can be oxidised by reducing manganese. This process follows Reed et al. (2011). The genereated iron-III immediately precipitates as iron oxyhydroxide.

Structural iron in clay minerals can be reoxidised as well. We only allow this process in the presence of oxygen, it transforms back to iron-III, which is kept bound in the clay minerals.

Hydrogen sulphide can reduce any of the previously mentioned oxidants, being converted to sulphate. The reaction with oxygen or nitrate is carried out as a two-step reaction. The intermediate species formed in these reactions is elemental sulphur, which can be further oxidised to sulphate. These processes follow the same kinetics as in the water column, see Section 2.4.5. Hydrogen sulphide can alternatively react with manganese oxides or iron oxyhydroxides, producing dissolved Mn-II or Fe-II. For the generated iron-II, we, however, assume either an immediate precipitation to iron monosulphide or an immediate absorption to clay minerals, whichever is more favourable. We assume these reactions to be proportional to both the concentration of sulphide and the metal oxides. Hydrogen sulphide can also reduce structural iron-III in the clay minerals, the iron-II will in this case remain in the clay.

Iron monosulphide is typically not directly oxidised but dissolves at low sulphide concentrations. However, if it is exposed to oxygen, we assume a complete oxidation to iron-III and sulphate.

Finally, pyrite can be oxidised in the presence of oxygen or manganese-IV, but in marine environments not by iron-III (Schippers and Jørgensen, 2002). We assume a complete oxidation to sulphate and iron oxyhydroxides.

2.6 Carbon cycle

The carbon cycle in this model is included in the typical way, following Millero (1995) and Dickson et al. (2007). Four measures describe the state of the carbonate system in the water:

- pH
- total alkalinity (TA)
- dissolved inorganic carbon concentration (DIC)
- CO_2 partial pressure (pCO_2)

Knowledge of any two of them allows the determination of the other two. We use TA and DIC as state variables. The reason for this is that both pH and pCO_2 can be changed by quick equilibrium reactions with a proton transition which occur faster than our model time step allows, while TA and DIC cannot. For details on these reactions, see Dickson et al. (2007).

As we are mainly interested in pH (for adsorption and precipitation reactions) and pCO_2 (for gas exchange with the atmosphere), we need to derive these from the state variables. This is done in an iterative procedure. Starting with a guessed pH value (from the last model time step), we calculate the fractionation of DIC into the different species (CO_2, HCO_3^-, CO_3^{2-}). From this, we determine a carbonate alkalinity. We do the same for other substances taking part in acid-base dissociation reactions (water, boron, sulphide, phosphate). The sum of all their alkalinities should then match the known total alkalinity, but a

Geosci. Model Dev. Discuss., https://doi.org/10.5194/gmd-2018-109
Manuscript under review for journal Geosci. Model Dev.
Discussion started: 2 May 2018

difference occurs because the approximated pH was incorrect. So we do a Newton iteration to find an improved pH estimate, using a fixed number of ten steps for a better parallel performance of the code.

2.7 Numerical aspects

The equations which determine the temporal evolution of the state variables are solved by a mode splitting method. Physical and biogeochemical processes are solved alternately in separate time steps.

2.7.1 Numerics of physical processes

Vertical diffusion is done explicitly by multiplying each vertical tracer vector by a diffusion matrix. This includes turbulent mixing in the water column as well as pore water diffusion, bioturbation (faunal solid transport) and bioirrigation (faunal solute transport). This diffusion matrix is tridiagonal, and for a small time step, which is in our case limited by the thin layers at the top of the sediment, a Euler-Forward method can be applied. Larger time steps could be split into smaller Euler-Forward steps, which means a repeated multiplication by the tridiagonal matrix. We instead use an efficient algorithm to calculate powers of the tridiagonal matrix (Al-Hassan, 2012), and perform the multiplication only once.

2.7.2 Numerics of biogeochemical processes

The sources and sinks for the different tracers are calculated from the process rates. These not only include biogeochemistry, but also parametrisations for lateral transport processes as well as sedimentation and resuspension.

To calculate the changes of a tracer concentration with time, we form the sum of the processes consuming or producing it (Radtke and Burchard, 2015).

$$\frac{\partial}{\partial t} T_i \quad = \quad \sum_k p_k \left(q_{ik} - s_{ik} \right) . \tag{5}$$

Here T_i represents the concentration of tracer i, p_k is the rate at which process k runs, and q_{ik} (and s_{ik}) is the stoichiometric ratio in which process k produces (or consumes) tracer i.

In order to ensure both non-negativity of the tracer concentrations and mass conservation, we apply the positive Euler-Forward method from Radtke and Burchard (2015). It is a clipping method which, in case of a tracer concentration becomes negative during one Euler-forward time step, first executes a partial time step until this tracer is zero. Then the rest of the time step is continued without the processes consuming this tracer, they are switched off. More than two partial time steps may be needed if more than one tracer is exhausted.

2.8 Automatic code generation

The model code is not hand-written. Instead, the model is described in a formal way in terms of its tracers, constants and processes in a set of text files. The model code is then generated by a "code generation tool" (CGT) which fills in this information into a code template file. The advantage is that the same biogeochemical equations can in this way be integrated into different

models. While the current version is written in Pascal, the three-dimensional version in MOM5 has been created as a Fortran code. The CGT is open-source software and can be downloaded at www.ergom.net.

3 Observed data used for model applications

We use three different observational datasets for model calibration and validation. The data used are (a) pore water profiles for different dissolved species, (b) sediment elemental composition, and (c) estimates of bioturbation intensity.

3.1 Selected stations

All data were collected at seven different stations in the Southern Baltic Sea, see Fig. 1. (We always present the stations from west to east.) The mud stations LB and MB are situated in the Mecklenburg Bight, a trough-like bay in the south-western Baltic Sea where salinities are up to 20. Stations ST and DS are on sandy substrate, the latter one is situated in only 22 m depth near the major sill which impedes the transport of the more saline North Sea water into the inner part of the Baltic Sea. Station AB is situated in the central Arkona Basin in 45 m depth. The Arkona Basin is the most western basin of the inner Baltic Sea. It accumulates organic matter not only from local primary production, but also laterally imported particles from coastal areas experiencing strong eutrophication, especially from the Oder River (Christiansen et al., 2002). Station TW is a silt station with a median grain size around 40 μm. The last station, the sandy station OB on the Oder Bank, is not a place of organic matter deposition, but rather of transformation before the detritus is transported to deeper locations. The Oder Bank is a shallow sandy area strongly influenced by the Oder river plume (Voss and Struck, 1997).

All the stations were sampled during twelve cruises between July 2013 and January 2016 to cover different seasons. However, not every station was sampled during every cruise. The calibration of the model was already started in parallel to the sampling campaign, such that only data from the first seven cruises (until January 2015) could be used for model fitting.

3.2 Pore water analyses

Short sediment cores with intact sediment-water interface were taken by a multicorer, a device which simultaneously extracts 8 sediment cores from the sea floor. Pore water was extracted at different depths by rhizones. For a detailed description of the analytical methods used, we refer to Lipka and Böttcher (in prep.). Here we just give a short summary: ammonium concentrations were measured onboard using standard photometric methods, e.g. (Winde et al., 2014). The quantification of major and trace elements was done on land, following the ICP-OES method (Kowalski et al., 2012). Dissolved inorganic carbon was measured by a mass spectrometer in the gas phase after a treatment of the pore water sample with phosphoric acid. Total alkalinity was determined colorometrically after Sarazin et al. (1999). Dissolved sulphide was determined spectrophotometrically by the methylene blue technique (Cline, 1969).

Geosci. Model Dev. Discuss., https://doi.org/10.5194/gmd-2018-109
Manuscript under review for journal Geosci. Model Dev.
Discussion started: 2 May 2018

Instead of directly comparing sulphate concentrations between model and reality, which change over time with salinity, we use the sulphate deficit defined as

$$\Delta SO_4 = [SO_4^*] \frac{[K]}{[K*]} - [SO_4] \ , \tag{6}$$

where $[SO_4]$ and $[K]$ are the measured concentrations of sulphate and potassium (regarded as passive tracer) in the pore water and $[SO_4^*]$ and $[K^*]$ are their typical concentrations in sea water of 35 g/kg salinity, Dickson and Goyet (1994).

3.3 Sediment composition

Parallel sediment cores from the same multicorer casts as used for the pore water analysis were subsampled in 1 cm steps, freeze-dried under vacuum and homogenised for geochemical analyses. Total carbon (TC) as well as nitrogen (TN) and sulphur (TS) contents were measured by combustion, chromatographical separation of the released gases and their determination with a thermal conductivity detector. The total inorganic carbon (TIC) content was measured by acidic removal of carbonates and analysis of the released CO2 with a nondispersive infrared detector. The total organic carbon (TOC) content was then calculated by the subtraction of TIC from TC values. At the sand stations (ST, DS and OB), the mass fractions were measured in the fine fraction (< 63 μm) of the sediment only, assuming that the coarse fraction does not contain these elements in a significant amount. So, the percentage in the whole sediment was calculated by multiplying with the fine fraction ratio that was determined by laser diffractometry. Analytical details on the used devices, their calibration as well as precision and accuracy can be obtained from Bunke (2018).

3.4 Bioturbation intensity estimates

In order to analyse bioturbation intensities (D_B), six to 24 cores per station were sliced onboard immediately after retrieval at 0.5 cm intervals to 3 cm depth and at 1 cm intervals to 10 cm for vertical chlorophyll-a (Chl-a) profiles. All samples were deep-frozen (-18°C) and stored until extraction (Sun et al., 1991). In the laboratory, the defrosted sediment samples were homogenised and three parallel subsamples of 1 cm^3 volume were taken from each slice. After adding 9 ml of 96% ethanol and an incubation period of 24 h in the dark, the sampled were centrifuged at 4000 rpm for 5 minutes, measured photometrically (663 and 750 nm) and chlorophyll was calculated based on HELCOM (1988). The vertical chlorophyll profiles were interpreted using the bio-mixing model developed by Soetaert et al. (1996b). Experimentally derived chlorophyll decay constants of 0.01 d^{-1} for mud and 0.02 d^{-1} for sand (Morys, 2016) and a sedimentation rate ω of 0.00001 cm d^{-1} were used. The model applied may distinguish between diffusive and non-diffusive mixing. The latter mode of bioturbation was neglected in our study despite the fact that it may be the dominant particle transport process in certain areas (e.g. AB).

4 Model setup and optimisation

There are three ways in which observations feed into our model. There are:

1. model constants which were derived in earlier studies and which our model adopted from previous models,

Geosci. Model Dev. Discuss., https://doi.org/10.5194/gmd-2018-109
Manuscript under review for journal Geosci. Model Dev.
Discussion started: 2 May 2018

Table 2. Site-specific data used as model input

station	porosity (rel. units)	sed. acc. rate (kg m^{-2} $year^{-1}$)	source of sed. acc. rate
LB	0.91	0.6	(Kersten et al., 2005)
MB	0.91	0.3	(Leipe et al., 2011)
ST	0.40	-	-
DS	0.40	-	-
AB	0.91	1.1	(Emeis et al., 2002)
TW	0.60	-	-
OB	0.40	-	-

2. initial and boundary conditions, determining tracer concentrations at the beginning and throughout the model run, and
3. calibration data which help to confine uncertain model parameters during a repeated model calibration process.

4.1 Use of data as model constants

Most of the observations which help confine our model processes enter our model indirectly, since model constants are inherited from ancestor models. Especially in van Cappellen and Wang (1996), a thorough confinement of model constants based on observations was achieved. We add to that by supplying site-specific observations for porosity for all seven stations, set to a homogeneous value per substrate type estimated from measurements within the SECOS Project (Lipka and Böttcher, in prep.). Also, sediment growth estimations for the three muddy sites are taken from different sources, as shown in Table 2.

4.2 Initial and boundary conditions

The initial conditions for most biogeochemical state variables in the water column are taken from a previous run of a three-dimensional ERGOM model (Radtke, unpublished), which contained a simplified sediment model as described e.g. in Radtke et al. (2012). Concentrations of sulphate and calcium were set to salinity-determined values as described by the standard composition of sea salt (Turekian, 1968). Dissolved dinitrogen was initialised at 100% saturation (Hamme and Emerson, 2004).

Fluff and sediment, in contrast, were initialised empty. We allowed them to fill up with material derived from the water column during the simulated period of 100 years. Since the model conserves nitrogen and phosphorus, the filling of the sediments would have led to a depletion in the water column. To overcome this, we relax the winter concentrations of dissolved inorganic nitrogen and phosphorus (DIN and DIP) against values obtained from the previous 3-d model run. This relaxation is applied every winter, so the nutrients required to fill the model domain are provided from an artificial external source. Their input is large at the beginning of the model run and decreases over time as the sediment reaches a state which is almost in equilibrium with the organic matter supply from the water column above.

Geosci. Model Dev. Discuss., https://doi.org/10.5194/gmd-2018-109
Manuscript under review for journal Geosci. Model Dev.
Discussion started: 2 May 2018

4.3 Model fit to observed data

Pore water profiles from Lipka (2018) were then used to calibrate the model. The calibration included optimizing model parameters for individual stations, as well as parameters for the whole model domain.

Typically, this type of calibration is done manually by the modeller. But due to the large number of parameters to optimise (115 in total), we decided to do a systematic, algorithm-based optimisation.

4.3.1 Penalty function

The first step in such an optimisation is to define a metric or a penalty function quantifying the misfit between model and observations. Our aim is then to minimise this function.

We chose to penalise the relative deviation between model and measurement and define the penalty function by

$$P = \sum_{i=1}^{i_{max}} \sum_{j=1}^{j_{max}(i)} r_{i,j}^2 \cdot w_i \,. \tag{7}$$

Here, i_{max} is the number of state variables we compare and $j_{max}(i)$ is the number of observations of this state variable in all depths and at all stations. The expression $r_{i,j}$ is a measure for the relative deviation between model value $m_{i,j}$ and observation $o_{i,j}$,

$$r_{i,j} = \log_{10}\left(\frac{m_{i,j}+\Delta_i}{o_{i,j}+\Delta_i}\right) . \tag{8}$$

The term Δ_i is included to avoid huge relative errors between values which are close to zero. It denotes the random deviation in this parameter, quantified from duplicate or triplicate measurements of the same parameter in different sediment cores of the same sampling. Obviously $r_{i,j}$ becomes zero if model and observations match. Finally, the weight w_i assigned to each comparison in equation (8) is defined as the ratio

$$w_i = \frac{\overline{o}_{i,j}}{\Delta_i} \tag{9}$$

between the average observed value of the variable and the random deviation. The weight is applied to make sure that fitting the most certain variables has the highest priority.

The pore water species which are fitted are: ammonium, phosphate, silicate, sulphide, iron, manganese, the total alkalinity, and the relative sulphate deficit[10].

4.3.2 Optimisation strategies

After we defined a penalty function, the second step is to choose an algorithm to minimise it. Several such algorithms exist, however, our choice of methods was restricted by the relatively long runtime of a single model iteration. Since it took about 8 minutes to run a single station for 100 years, we had to choose methods which

[10] defined as $\Delta SO_4\,[K^*] \,/\, \left(\left[SO_4^*\right]\,[K]\right)$, see eq. 6

1. needed a relatively small number of iteration steps and therefore
2. allowed for a high degree of parallelism in the individual optimisation step, in order to effectively search the 115-dimensional parameter space.

Our first choice was the AHR-ES algorithm, implemented in the R-Package calibraR (Oliveros-Ramos and Shin, 2016). As a genetic algorithm, it considers each vector of model parameters as a genome of an individual. A low value of the penalty function is then considered as a good fitness of the individual. The iteration is then performed in the three steps as follows:

1. selection, where only the best currently known vectors are selected,
2. recombination, where their genome is combined to produce children, and
3. mutation, where their genome is randomly modified, following certain algorithm-specific rules.

The AHR-ES algorithm is special in the sense that the recombination step produces just one "child", combining the parameter vectors of all surviving individuals in a weighted mean. To calculate these weights, the algorithm takes advantage of not only determining one value of fitness, but rather different "fitnesses" for matching different observations. High weights are then assigned to those genome parameters that influence the output parameters most in which the individual has a high fitness. This optimally breeded child is then cloned several times and, after mutation of the clones, forms the starting population for the next step.

We used 200 "individuals", each consisting of seven single models for the seven different stations run in parallel, and optimised them over 120 generations. We were, however, not satisfied with the optimisation result. Possibly we just failed to find out the optimal settings for the algorithm, such as the survival rate.

Our second choice was a simple alternative algorithm: our own extension of the Generalised Pattern Search (GPS) algorithm (Hooke and Jeeves, 1961). Every optimisation step consists of two sub-steps. The first substep is the most simple "grid search" step in which all 115 parameters are varied by a predefined step width. We run 230 sets of 7 models in parallel, such that each parameter can be both increased and decreased. In the second substep, 230 combinations of the most successful changes are formed. Even if no single-parameter change could improve the existing solution, sometimes combinations of them can, which is the basic idea of GPS. The parameter vector with the best score which was obtained in any of the two substeps is then chosen as the starting point for the next step. If none of the two sub-steps lead to an improvement of the overall fit, the step size is reduced by a factor of 2.

The optimisation converged after 30 iteration steps and reduced the error function from 6363 (the value obtained by previous manual tuning) to 4797.

The algorithm obviously does not guarantee that we reach a global optimum, which can be seen as a drawback. However, in a vector space with a dimension as high as ours, it is anyway hard to find a non-local point with a better score, no matter if it is by manual optimisation or a different search algorithm.

Geosci. Model Dev. Discuss., https://doi.org/10.5194/gmd-2018-109
Manuscript under review for journal Geosci. Model Dev.
Discussion started: 2 May 2018

4.4 Manual correction of sand and silt stations

For the sand stations and the single silt station, the automatic optimisation resulted in an unrealistic set of parameters. The estimated bioirrigation rates were estimated as low as those of the mud stations. However, at these low bioturbation rates, the sediments failed to accumulate realistic amounts of organic matter. The pore water profiles we obtained, however, seemed to match relatively well with the observations. But the realistically low concentrations of solute species were obtained by keeping detritus out of the sediments. The model assumed relatively high rates of lateral removal of fluff, such that only a small fraction of the locally produced detritus was actually processed in the sediments.

This illustrates the problem that if the diffusivity is unknown, very different transports can be caused by the same pore water gradient. We therefore decided to manually modify the solution by (a) reducing the fraction of detritus removed from the fluff layer by lateral transport and (b) enhancing bioturbation and bioirrigation rates, both by the same factor. This led to similar pore water profiles, but higher turnover rates and organic content in the sediments.

5 Model results and validation

5.1 Comparison to measured pore water profiles

In this section, we compare and discuss observed and simulated pore water profiles of several chemical species relevant for early diagenetic processes. Model results are taken from the last year of the 100-year simulation, which was driven by a repeated forcing every year. After this simulated period, the model almost reached a quasi-steady state, which means the annual cycle of pore water concentrations was nearly repeated year after year at each of the stations. The sixth class of detritus, in contrast, which we defined as non-degradable, did not reach a stable concentration, but continued to accumulate in the sediment during the period of 100 years. But this continued accumulation did not influence the pore water profiles due to the fact that it was assumed bioinert.

5.1.1 Pore water profiles at mud stations

Figure 4 shows a comparison of simulated and measured pore water profiles at the three mud stations. The curves show the annual average pore water concentrations simulated by the model, while the shaded areas give the range in which each parameter varies throughout the year. Horizontal lines indicate the range of measurements over all cruises within the project.

In the left panels, we see that the rise of alkalinity with depth is captured well by the model, except for the AB site where observations show a higher alkalinity below 10cm depth. The decline in sulphate follows the lower range of the observations.

The panels in the second column show that also the vertical profiles of ammonium and silicate are represented relatively well by the model. However, especially at the Arkona Basin station, the observed range of both ammonium and sulphide shows a strong variation (by an order of magnitude). The model does not capture that but rather sticks to the lower range of the observations. Most probably, the variability in the observations is not due to seasonality, but a consequence of spatial variability between sampling sites, since the samples were taken from two sites 23 km apart.

Surprisingly, the model is able to reflect the differently steep sulphide profiles between the stations LB and MB. While (Lipka and Böttcher, in prep.) sees the low sulphide concentrations which occur especially in March 2014 at MB as an indication for a preceding mixing event, our model cannot adopt this interpretation due to its limitation to a temporally constant vertical mixing. In contrast, our model suggests a higher deposition of iron oxyhydroxides at this site.

The right panels show that the modelled manganese concentrations match the observations quite well. The dissolved iron profiles show their maxima at the correct depths and a relatively large seasonal spread. The measurements show an even larger spread than the model. For the phosphate profiles, the model results mostly resemble the lowest of the measured values. This can be seen as an artefact of our fitting method, more precisely of the choice of our penalty function. Giving a penalty for the relative error means that the same absolute error is punished heavier if the observation was smaller, making the model try harder to fit low values compared to high ones.

The model results for the mud stations fit quite well, considering the fact that the real pore water profiles may be shaped by very different temporal variations. These include, for example, mixing events, changing loads of organic matter or temperature and salinity variations. Our model, not knowing the sediments' past, can only try to estimate the average conditions that might produce similar pore water concentrations.

5.1.2 Pore water profiles at sand stations

Figure 5 illustrates the model fits at the sandy stations.

All of the sandy stations have one major error in common: sulphide concentrations are strongly overestimated at depths below 5 cm. We suppose that the precipitation or reoxidation of sulphide are underestimated. For all other pore water species, the agreement between measured and modelled ranges is reasonable. Especially the rise of alkalinity with depth is captured well by the model. The sulphate deficit in the empirical data has a large uncertainty, as it is calculated as a small difference of similarly large quantities..

In our model, the sandy sites show a more pronounced seasonal cycle in the pore water profiles compared to the muddy stations. Especially iron and manganese concentrations vary considerably due to the seasonally different supply of quickly degradable organic matter and correspondingly differences in mixing intensity. While the variability in the supply of fresh organic matter is captured by the model, the variation in mixing is not. Still, the simulated ranges are supported by the variability in the observed pore water concentrations.

5.1.3 Pore water profiles at the silt station Tromper Wiek

For the station Tromper Wiek, we used data from two different cruises, in April and June 2014. Even if the idea in the SECOS project was to repeatedly sample the same station, the locations were approximately 6 km apart for this station, and the substrate type at the station sampled in April was sand rather than silt. The amount of sulphide in the pore waters showed a large difference between the April and the June cruise, the latter concentrations exceeding the former by a factor of 20. This reflects spatial rather than temporal variations. Some of the depth intervals were only sampled in the June cruise, which explains the different observed ranges at the different depths.

Geosci. Model Dev. Discuss., https://doi.org/10.5194/gmd-2018-109
Manuscript under review for journal Geosci. Model Dev.
Discussion started: 2 May 2018

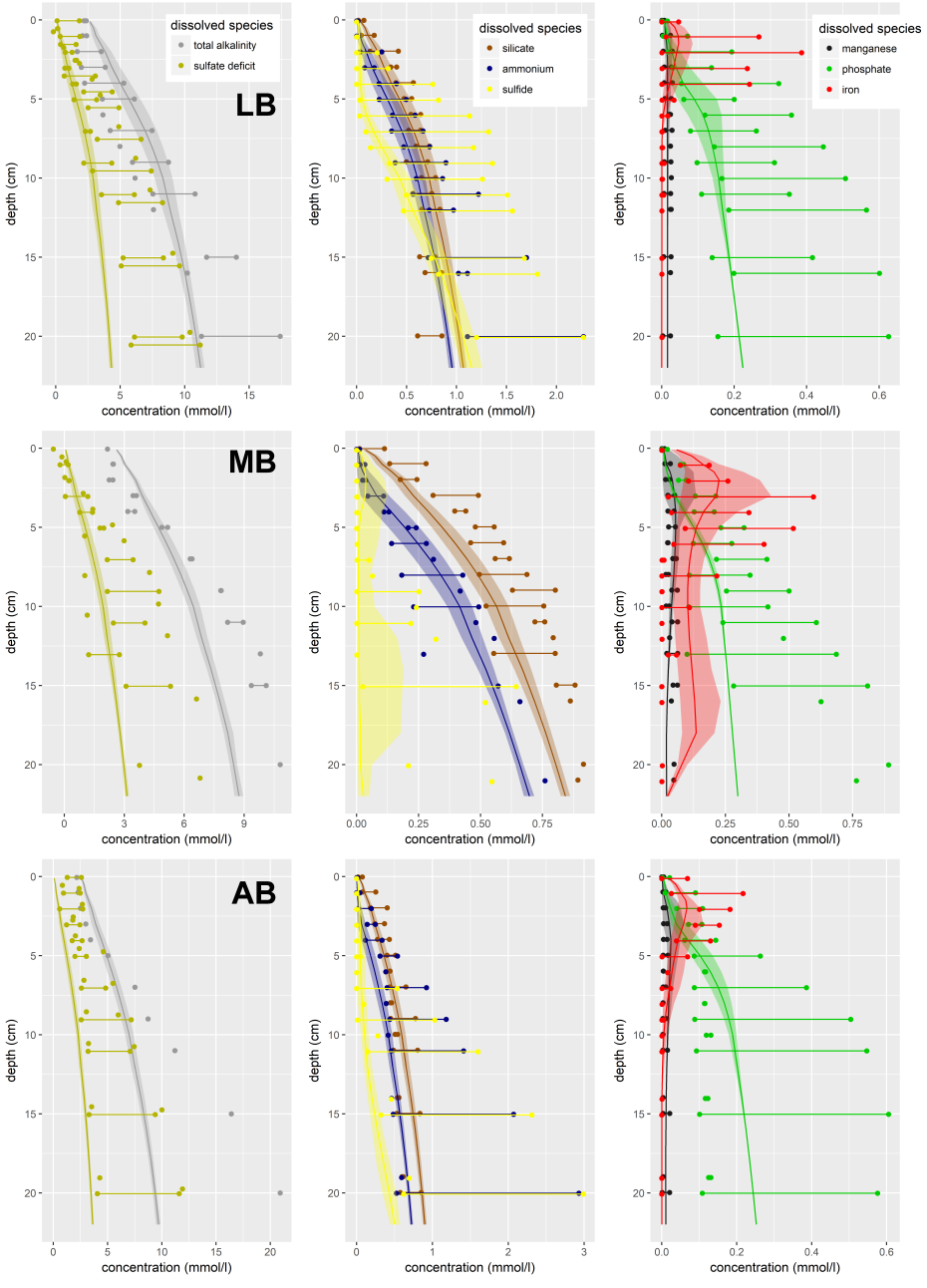

Figure 4. Pore water concentrations of several dissolved species at the three mud stations Lübeck Bight (top row), Mecklenburg Bight (middle row) and Arkona Basin (bottom row). Points and horizontal lines indicate the range of measurements. Curves and shading present the model results and indicate year-average concentrations and the seasonal range. Please note the different horizontal scales.

Geosci. Model Dev. Discuss., https://doi.org/10.5194/gmd-2018-109
Manuscript under review for journal Geosci. Model Dev.
Discussion started: 2 May 2018

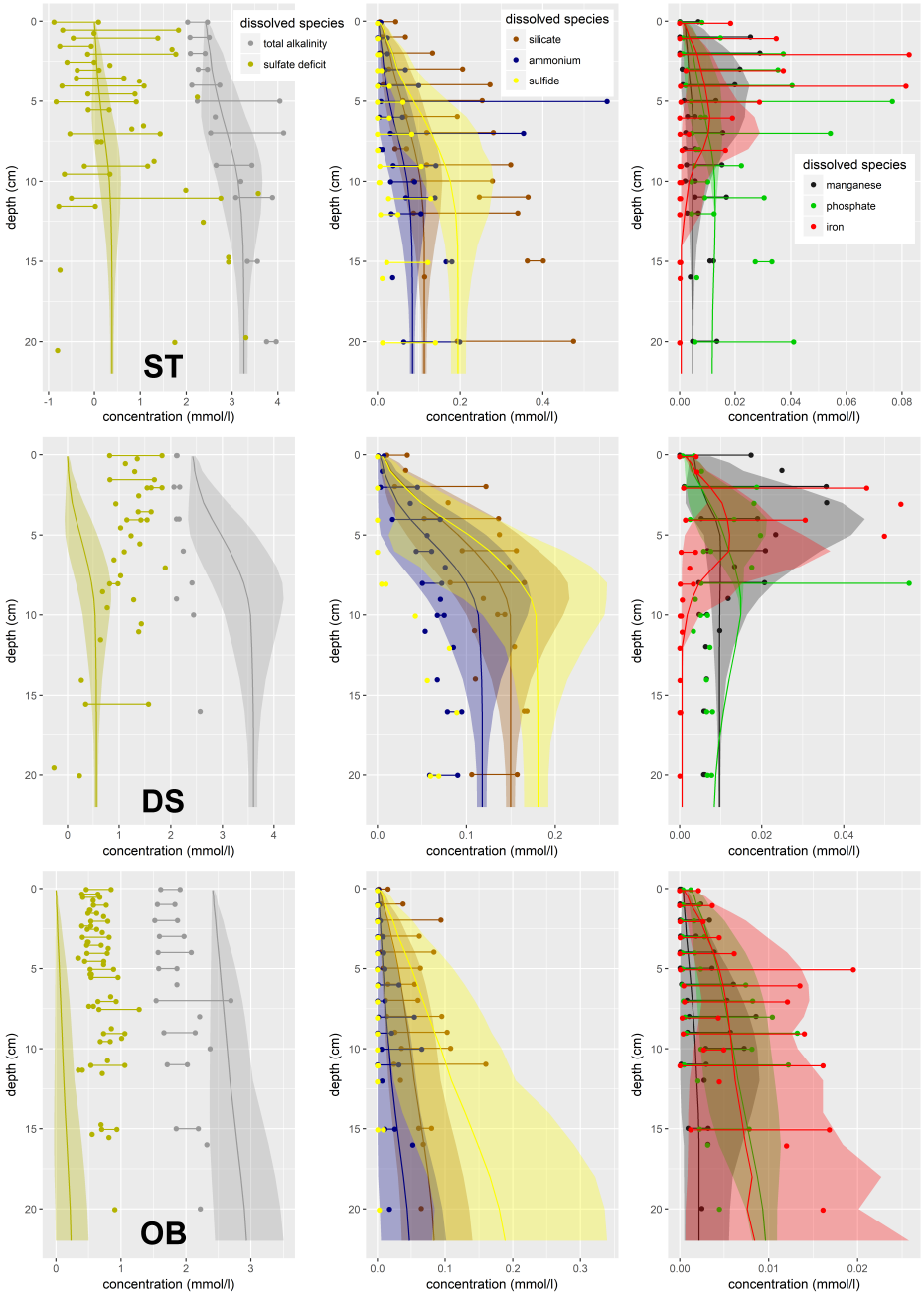

Figure 5. Pore water concentrations of several dissolved species at the three sand stations Stoltera (top row), Darss Sill (middle row) and Oder Bank (bottom row). Points and horizontal lines indicate the range of measurements. Curves and shading present the model results and indicate year-average concentrations and the seasonal range. Please note the different horizontal scales.

Geosci. Model Dev. Discuss., https://doi.org/10.5194/gmd-2018-109
Manuscript under review for journal Geosci. Model Dev.
Discussion started: 2 May 2018

Geoscientific Model Development Discussions
Open Access
EGU

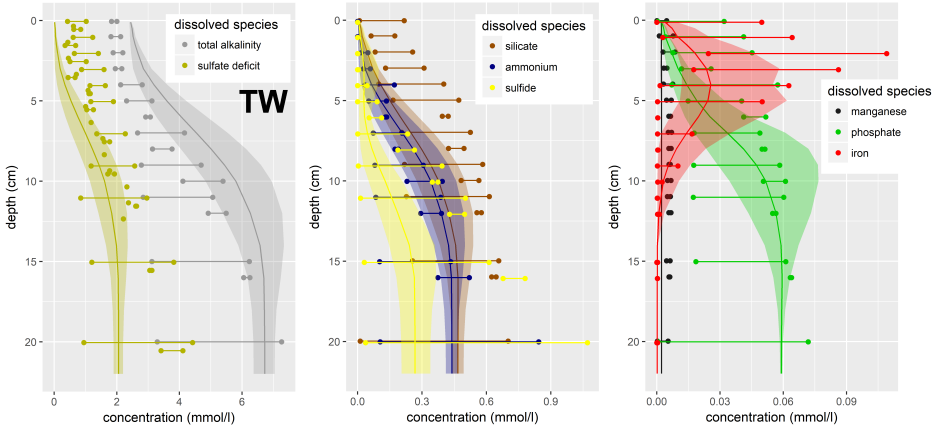

Figure 6. Pore water concentrations of several dissolved species at the silt station Tromper Wiek. Points and horizontal lines indicate the range of measurements. Curves and shading present the model results and indicate year-average concentrations and the seasonal range.

The good agreement in the profiles of ammonium and phosphate (middle panel in Fig. 6) suggests that total mineralisation is captured well. The left panel shows that the model estimates the sulphate deficit at the higher range of observations, but the rise of alkalinity with depth at the lower range.

The model overestimates the vertical extent of iron-II in the pore waters. However, the model correctly reproduced the range of iron concentrations, and also the fact that dissolved manganese concentrations were always low compared to those of iron.

5.2 Comparison to sediment composition estimates

In Figure 7, we compare the composition of the solid parts of the sediment between model and measurements. The fraction of nitrogen, sulphur and total organic carbon (TOC) in the total mass of the dry sediment is shown for all seven stations.

We see that for the mud stations LB and MB, the modelled element concentrations show a quantitative agreement with the measurements. The main difference is that the measured values show strong vertical fluctuations, which may be the result of the deposition history. In the mud station AB (Arkona Basin), however, the actual concentrations of all three elements are heavily underestimated. Nonetheless, the depth gradients of the concentrations match quite well, so there is perhaps just a constant offset. This might be caused by the accumulation of bioinert organic material, possibly of terrigenous origin from the Oder river.

In all sand stations (ST, DS, OB), the amount of sulphur in the sediments is underestimated. The observed sulphur in the sediments varies with depth and shows a maximum at around 10 cm depth. The fact that sulphide, in contrast, was overestimated in the pore waters, suggests that the precipitation of sulphide may be underestimated in the sandy cores.

N and TOC are present in realistic quantities at the OB station. At the other two sand stations, the N and TOC observations show maxima at the top (station DS) or bottom (station ST) of the profile, which are not captured by the model. These are most likely the traces of past sedimentation or bioturbation events.

Geosci. Model Dev. Discuss., https://doi.org/10.5194/gmd-2018-109
Manuscript under review for journal Geosci. Model Dev.
Discussion started: 2 May 2018

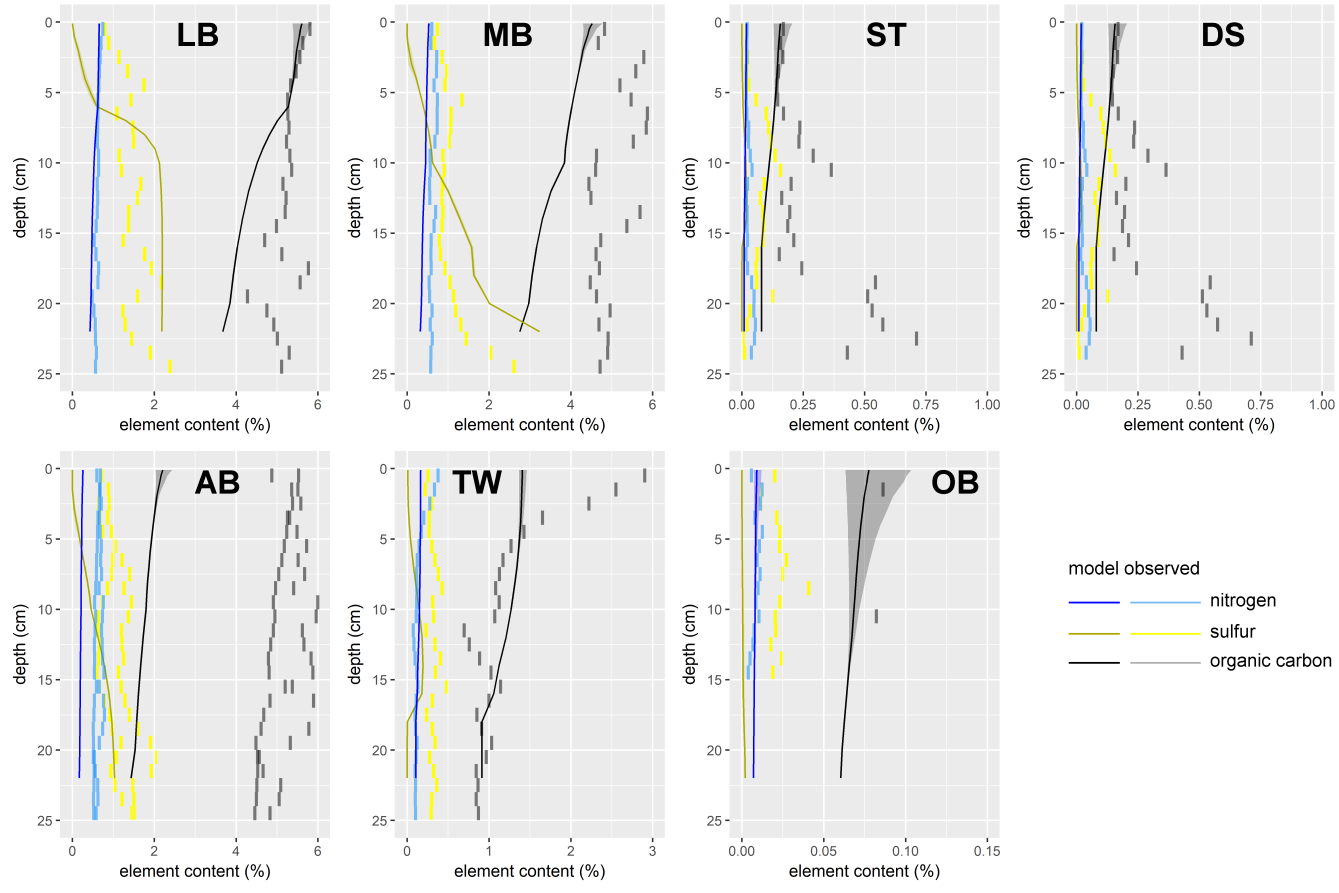

Figure 7. Mass fractions of nitrogen, sulphur and organic carbon in the dry sediment, model results (curves and shading for seasonal range) versus measurements (vertical segments). Please note that the scales on the horizontal axes differ by a factor of 40.

5.3 Comparison to measured bioturbation intensities

The empirically estimated bioturbation intensities span a large range at each station. A reason for this may be that while our model assumes a temporally constant bioturbation, in reality it is highly variable. Mixing events by animals or shear stress alternate with periods without mixing. Investigations of individual cores can only give snapshots of this highly variable mixing rate.

Figure 8a shows a comparison of measured bioturbation diffusivities D_B and to those used in the model. Since the observed ranges are very large, they almost always contain the value assumed in the model. An exception is the Tromper Wiek site where exceptionally high D_B values were measured. This may, however, be an artefact based on the method calculating the diffusivities. While in the model, we assume diffusion-analogue mixing, in nature also non-local mixing occurs. The two processes can be distinguished from the analysis of Chl-a profiles. Figure 8b shows how often the samples from a specific site

Geosci. Model Dev. Discuss., https://doi.org/10.5194/gmd-2018-109
Manuscript under review for journal Geosci. Model Dev.
Discussion started: 2 May 2018

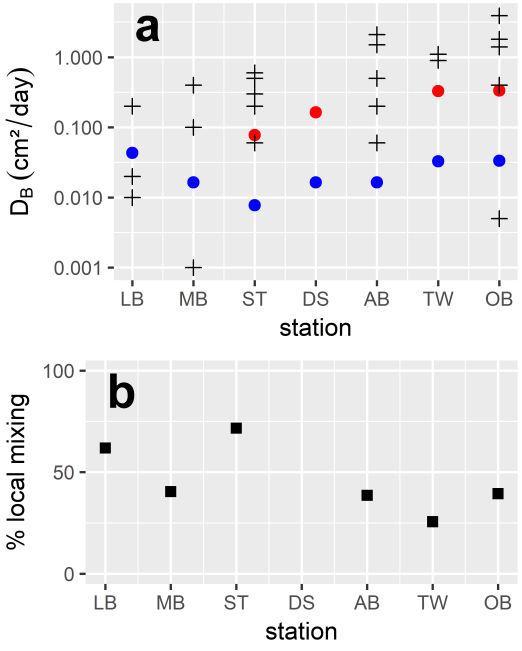

Figure 8. (a) Model estimations (blue dots), manually corrected for sand and silt stations (red dots) and Chl-a-based estimates (black crosses) for bioturbation intensity. Black crosses represent averages over all cores from a single month where the Chl-a profiles in the sediment supported the assumption of diffusion-analogue mixing. So, variation can be interpreted as temporal variability. (b) The percentage of the cores for which a local, diffusion-analogue mixing process could explain the observed Chl-a profiles.

supported the hypothesis of diffusion-analogue mixing. For the station TW, it was only one fourth of the sediment cores that could be explained assuming local mixing, so non-local mixing was identified as a major process here. D_B values were only calculated for cores where the observed Chl-a profiles could be explained by local mixing alone.

The automatic model calibration yielded diffusivities at the sand and silt stations which were as low as those at the mud stations. Such a weak mixing, however, could not supply enough organic matter to the sediments to reach measured element compositions. Therefore, they were corrected upwards, resulting in higher mixing at the sandy than at the muddy sites. This agrees with recent estimates of bioturbation potential (Gogina et al., 2017; Morys et al., 2017), an index describing the ability of macrofauna to displace the sediment particles, resulting in a mixing effect. This potential was estimated to be higher in the more shallow sandy areas than in the muds. Also, measured bioturbation rates in the SECOS project were higher in the sands than in the muds (Morys, in prep.). However, the high variability of bioturbation rates within stations makes it difficult to prove a significant difference in D_B between sandy and muddy areas empirically (Morys et al., 2016).

Geosci. Model Dev. Discuss., https://doi.org/10.5194/gmd-2018-109
Manuscript under review for journal Geosci. Model Dev.
Discussion started: 2 May 2018

6 Conclusions

In this manuscript, we described an integrated model for ocean biogeochemistry. It simulates ocean biogeochemistry both in the water column and in the sediments.

The model was obtained by combining its two ancestor models, the water column model ERGOM (Neumann, 2000), and the early diagenetic model used in Reed et al. (2011). A few modifications were made to the existing models, partly to include additional processes relevant for the area of interest, the German EEZ in the Baltic Sea. These model extensions include

- closing the carbon cycle in the sediments which allows the determination of pH,
- adding a specific numerical scheme for the diffusion of the tracer "total alkalinity",
- using ion activities rather than concentrations to determine precipitation and dissolution potentials, allowing us to account for salinity differences,
- the explicit description of adsorption to clay minerals, and
- an alternative pyrite formation pathway via H_2 formation.

An automated model calibration approach was used to fit the model to pore water observations at seven sites in the study area. It was successful for the mud stations, but underestimated bioturbation rates and consequently the organic content of the sediment at the sand and silt sites. Therefore, these model parameters were adjusted manually at the sand and silt sites.

This issue illustrates a general problem related to models of this complexity. The large quantity of unknown model parameters results in many degrees of freedom, and different types of observations are needed to constrain them. Even so, a good fit to a constrained set of observations does not guarantee that the model dynamics are captured realistically.

We showed a comparison to three different kinds of observations, which in most cases showed good agreement. An exception was the strong overestimation of sulphide concentrations in sandy sediment pore waters. This most likely points to the underestimation of sulphide precipitation/reoxidation.

The analysis we showed suggests that the processes most relevant for these observations are adequately represented in the model. This does not include all parts of the model. For example, the nitrogen cycle was not compared to observations, which is due to the fact that the project SECOS in which this work was done did not focus on it.

Applying the model in a three-dimensional framework will reduce the degrees of freedom. For example, our model includes parametrisations for (a) lateral removal of fluff material from the sand stations and (b) lateral import of organic material at the mud stations. In a 3-d ocean model, these become intrinsically linked by the constraint of mass conservation. Other degrees of freedom arise from the supply of oxidised iron and manganese to the individual stations. In a 3-d model, the supply and distribution of these substances would be controlled by erosion and deposition and thus determined by the model physics.

Apart from these constraints, the implementation of the model in a 3-d framework is straightforward. Physically, the coupling between different locations would be controlled by the fluff layer, by its erosion and redeposition. Technically, the coupling is simplified due to the use of automatic code generation. Describing the model processes and constants in a formal way, keeping

them separate from code for specific models, means it is easy to switch between different "host models". The major difficulty in going 3-d is the limited amount of validation data, such as pore water profiles, compared to the strong spatial and temporal variability. A first step is the application of the model to the limited area of the German EEZ for which the model is calibrated.

In the long term, biogeochemical ocean models should aim at a process-resolving description of surface sediments. This is especially true for shallow ocean areas where the efflux of nutrients from the sediment strongly influences water column biogeochemistry, like in our study area. The magnitudes of denitrification and phosphate retention, or the spatial and seasonal patterns in which oxygen consumption occurs, may strongly influence marine ecosystems.

Very often, model studies discussing "what if"-scenarios use a relatively simple sediment representation. This includes studies on nutrient abatement, human-induced stresses on ecosystems (e.g. by fish farming) or climate sensitivity analyses. But the use of a present-day parameterisation for future scenarios means a neglect of possible changes. In the context of limited data and process understanding, this implicit "no change"-assumption may be the best we can presently do. But we should be aware of the uncertainty which is introduced by this pragmatic choice. Studying the sensitivity of sediment functions to external drivers in a process-resolving sediment model can be a way to quantify these uncertainties, and possibly derive an ensemble of alternative future parametrisations.

Code and data availability. A source code version of the model is provided in the supplement to this article. It includes the initial conditions and physical forcing files required to reproduce the obtained results.

The code is not hand-written, but can be generated automatically from a set of text files describing the model biogeochemistry, and a code template containing the physical and numerical aspects of the model code. All three required ingredients to obtain the model source code (the text files, the code template, and the code generator program) are also included.

These components in their current and previous versions are GPLv3 licensed and can also be downloaded from our website www.ergom.net.

For the calibration and validation data used in this study, we refer to the following publications: The pore water data can be found in Lipka (2018). The sediment composition data are published in Bunke (2018). The bioturbation rate estimates are available in Morys (in prep.).

Appendix A: Stoichiometric composition of model state variables

The stoichiometric composition of the model tracers is shown in Table A1.

Appendix B: Quantitative influence of different model extensions

Here we use a set of sensitivity experiments to illustrate how the model refinements introduced by us influence the results. In each of these, we switch off one of our model improvements. This means that we use three simplified model versions, in which

1. total alkalinity always diffuses with the bicarbonate diffusivity, no matter how many hydroxide ions contribute to it which, in reality, diffuse faster,

2. the saturation indexes for precipitation/dissolution reactions are calculated neglecting the (salinity-dependent) activity coefficients, and

3. the adsorption of ammonium, phosphate and iron onto clay minerals, as well as their reducible iron-III content, are neglected.

As an example, we apply these reduced models to the mud station AB.

The results are shown in Fig. A1 in dashed lines and compared to the full model. All modifications affect the dissolved concentrations of iron in different directions. This is probably because both pore water pH and the activity coefficients influence the precipitation to iron monosulphide. The third modification (adsorption to clay minerals) reduces the phosphate concentrations in the pore water. All other pore water species remain virtually unchanged by our model modifications.

Competing interests. No competing interests are present.

Acknowledgements. This study is embedded in the KÜNO Project SECOS (03F0666A) funded by the German Federal Ministry for Education and Research (BMBF). The model optimisation runs were performed on the HLRN supercomputing center. Free software which supported this work includes R/RStudio and Freepascal Lazarus. Marko Lipka and Michael E. Böttcher wish to thank I. Schmiedinger, A. Köhler and I. Scherff for their invaluable help in the laboratory. They also wish to express their gratitude to B. Liu for helpful discussions on transport processes.

Geosci. Model Dev. Discuss., https://doi.org/10.5194/gmd-2018-109
Manuscript under review for journal Geosci. Model Dev.
Discussion started: 2 May 2018

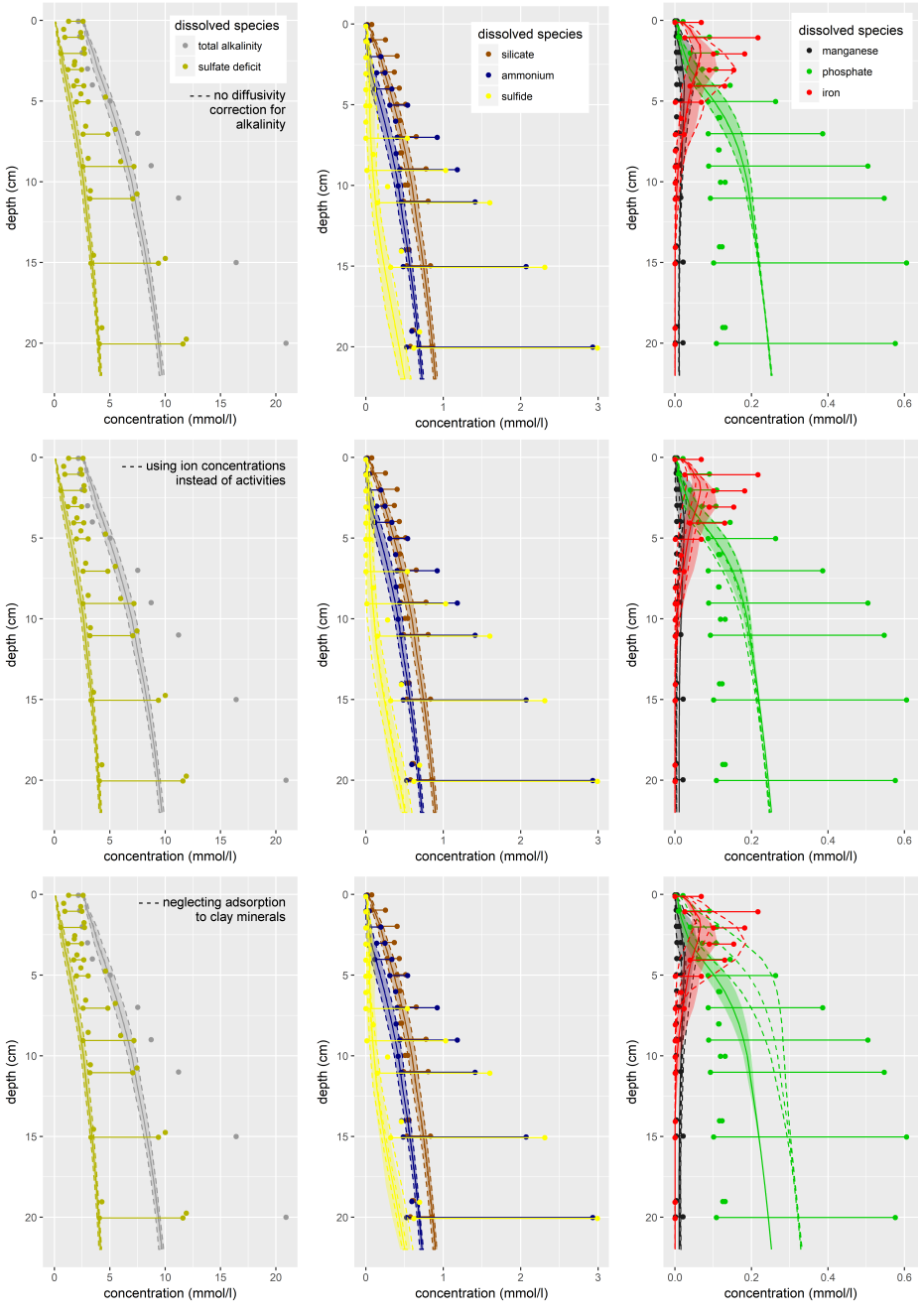

Figure A1. Pore water concentrations of several dissolved species at the mud station Arkona Basin. Points and horizontal lines indicate the range of measurements. Solid curves and shading present the model results and indicate year-average concentrations and the seasonal range. Dashed curves show the same, but for a model version which neglects one of our improvements: Top row - without correcting the diffusivity of total alkalinity for hydroxide ions. Middle row - without correcting the solute concentrations by activity coefficients. Bottom row - without assuming adsorption to clay minerals.

Geosci. Model Dev. Discuss., https://doi.org/10.5194/gmd-2018-109
Manuscript under review for journal Geosci. Model Dev.
Discussion started: 2 May 2018

Geoscientific Model Development Discussions
Open Access
EGU

Table A1. stoichiometric composition of tracers

tracer	C	Ca	Fe	H	Mn	N	O	P	S	Si	electric charge
t_no3						1	3				-1
t_lpp	6.625			16.4375		1	6.875	0.0625			
t_spp	6.625			16.4375		1	6.875	0.0625			
t_cya	6.625			16.4375		1	6.875	0.0625			
t_zoo	6.625			16.4375		1	6.875	0.0625			
t_det_?	9.9375			23.0625		1	9.9375				
t_detp_?				0.28125			0.375	0.09375			
t_don				4		1					+1
t_poc	1			2			1				
t_ihw			1	3			3				
t_ipw			1				4	1			
t_mow					1		2				
t_n2						2					
t_o2							2				
t_dic	1						2				
t_nh4				4		1					+1
t_no3						1	3				-1
t_po4							4	1			-3
t_h2s				1					2		
t_sul									1		
t_so4							4		1		-2
t_fe2			1								+2
t_ca2		1									+2
t_mn2					1						+2
t_sil				4			4			1	
t_ohm_quickdiff				1			1				-1
t_ohm_slowdiff				1			1				-1
t_sed_?	9.9375			23.0625		1	9.9375				
t_sedp_?				0.28125			0.375	0.09375			
t_ihs			1				3				
t_ihc			1				3				
t_ips			1				4	1			
t_ims			1						1		
t_pyr			1						2		
t_mos					1		2				
t_rho	1.6	0.6			1		4.8				
t_i3i			1	3			3				
t_iim			1	2			2				
t_pim				3			4	1			
t_aim				3		1					
h2o				2			1				
h3oplus				3			1				+1
ohminus				1			1				-1
i2i			1	2			2				

Tracer t_alk has been omitted since it just accumulates the changes to other tracers.

References

Al-Hassan, Q.: On Powers of Tridiagonal Matrices with Nonnegative Entries, Journal of Applied Mathematical Sciences, 6, 2357–2368, 2012.

Andersson, A., Haecky, P., and Hagström, Å.: Effect of temperature and light on the growth of micro-nano-and pico-plankton: impact on algal succession, Marine Biology, 120, 511–520, 1994.

Arndt, S., Jørgensen, B. B., LaRowe, D. E., Middelburg, J. J., Pancost, R. D., and Regnier, P.: Quantifying the degradation of organic matter in marine sediments: A review and synthesis, Earth-Science Reviews, 123, 53–86, doi:10.1016/j.earscirev.2013.02.008, 2013.

Bale, A. J. and Morris, A. W.: Organic carbon in suspended particulate material in the North Sea: Effect of mixing resuspended and background particles, Continental Shelf Research, 18, 1333–1345, doi:10.1016/S0278-4343(98)00046-6, 1998.

Belmans, F., van Grieken, R., and Brügmann, L.: Geochemical characterization of recent sediments in the Baltic Sea by bulk and electron microprobe analysis, Marine chemistry, 42, 223–236, 1993.

Boesen, C. and Postma, D.: Pyrite formation in anoxic environments of the Baltic, American Journal of Science, 288, 575–603, 1988.

Boudreau, B. P.: Diagenetic models and their implementation, vol. 505, Springer Berlin, 1997.

Bruckner, C. G., Mammitzsch, K., Jost, G., Wendt, J., Labrenz, M., and Jürgens, K.: Chemolithoautotrophic denitrification of epsilon-proteobacteria in marine pelagic redox gradients., Environmental microbiology, 15, 1505–1513, doi:10.1111/j.1462-2920.2012.02880.x, 2013.

Böttcher, M. E.: Experimental dissolution of CaCO3-MnCO3 solid solutions in CO2-H2O solutions at 20° C: I. Synthetic low-temperature carbonates, Solid state ionics, 101, 1263–1266, 1997.

Böttcher, M. E. and Dietzel, M.: Metal-ion partitioning during low-temperature precipitation and dissolution of anhydrous carbonates and sulphates, no. 10 in EMU Notes in Mineralogy, pp. 139–187, Mineralogical Society, 2010.

Bunke, D.: Sediment mixing processes and accumulation patterns in the south-western Baltic Sea, Ph.D. thesis, University of Greifswald (Germany), Greifswald, https://nbn-resolving.org/urn:nbn:de:gbv:9-opus-20780, 2018.

Butenschön, M., Clark, J., Aldridge, J. N., Allen, J. I., Artioli, Y., Blackford, J., Bruggeman, J., Cazenave, P., Ciavatta, S., Kay, S., and others: ERSEM 15.06: a generic model for marine biogeochemistry and the ecosystem dynamics of the lower trophic levels, Geoscientific Model Development, 9, 1293–1339, 2016.

Cahill, B., Radtke, H., and Neumann, T.: The role of coastal sediments for water column dynamics in the Western Baltic Sea, in prep.

Capet, A., Meysman, F. J. R., Akoumianaki, I., Soetaert, K., and Grégoire, M.: Integrating sediment biogeochemistry into 3D oceanic models: A study of benthic-pelagic coupling in the Black Sea, Ocean Modelling, 101, 83–100, doi:10.1016/j.ocemod.2016.03.006, 2016.

Christiansen, C., Edelvang, K., Emeis, K., Graf, G., Jähmlich, S., Kozuch, J., Laima, M., Leipe, T., Löffler, A., Lund-Hansen, L. C., Miltner, A., Pazdro, K., Pempkowiak, J., Shimmield, G., Shimmield, T., Smith, J., Voss, M., and Witt, G.: Material transport from the nearshore to the basinal environment in the southern Baltic Sea: I. Processes and mass estimates, Journal of Marine Systems, 35, 133–150, doi:10.1016/S0924-7963(02)00126-4, 2002.

Cline, J. D.: Spectrophotometric determination of hydrogen sulfide in natural waters, Limnology and Oceanography, 14, 454–458, 1969.

Davies, C. W.: The extent of dissociation of salts in water. Part VIII. An equation for the mean ionic activity coefficient of an electrolyte in water, and a revision of the dissociation constants of some sulphates, Journal of the Chemical Society (Resumed), 0, 2093–2098, doi:10.1039/JR9380002093, 1938.

Deutsch, B., Forster, S., Wilhelm, M., Dippner, J. W., and Voss, M.: Denitrification in sediments as a major nitrogen sink in the Baltic Sea: an extrapolation using sediment characteristics, Biogeosciences, 7, 3259–3271, doi:10.5194/bg-7-3259-2010, 2010.

Dickson, A. G. and Goyet, C.: Handbook of methods for the analysis of the various parameters of the carbon dioxide system in sea water. Version 2, Tech. rep., Oak Ridge National Lab., TN (United States), 1994.

Dickson, A. G., Sabine, C. L., and Christian, J. R.: Guide to best practices for ocean CO2 measurements., Tech. Rep. PICES Special Publication 3, PICES, Victoria, Canada, 2007.

Drobner, E., Huber, H., Wächtershäuser, G., Rose, D., and Stetter, K. O.: Pyrite formation linked with hydrogen evolution under anaerobic conditions, Nature, 346, 742, 1990.

Edzwald, J. K., Toensing, D. C., and Leung, M. C.-Y.: Phosphate adsorption reactions with clay minerals, Environmental Science & Technology, 10, 485–490, 1976.

Emeis, K., Christiansen, C., Edelvang, K., Jähmlich, S., Kozuch, J., Laima, M., Leipe, T., Loeffler, A., Lund-Hansen, L.-C., Miltner, A., and others: Material transport from the near shore to the basinal environment in the southern Baltic Sea: II: synthesis of data on origin and properties of material, Journal of Marine Systems, 35, 151–168, 2002.

Emeis, K.-C., Struck, U., Leipe, T., Pollehne, F., Kunzendorf, H., and Christiansen, C.: Changes in the C, N, P burial rates in some Baltic Sea sediments over the last 150 years—relevance to P regeneration rates and the phosphorus cycle, Marine Geology, 167, 43–59, 2000.

Engel, A.: Direct relationship between CO2 uptake and transparent exopolymer particles production in natural phytoplankton, Journal of Plankton Research, 24, 49–53, doi:10.1093/plankt/24.1.49, 2002.

Gadani, D. H., Rana, V. A., Bhatnagar, S. P., Prajapati, A. N., and Vyas, A. D.: Effect of salinity on the dielectric properties of water, Indian Journal of Pure & Applied Physics, 50, 405–410, 2012.

Gogina, M., Morys, C., Forster, S., Gräwe, U., Friedland, R., and Zettler, M. L.: Towards benthic ecosystem functioning maps: Quantifying bioturbation potential in the German part of the Baltic Sea, Ecological Indicators, 73, 574–588, doi:10.1016/j.ecolind.2016.10.025, 2017.

Guisasola, A., Jubany, I., Baeza, J. A., Carrera, J., and Lafuente, J.: Respirometric estimation of the oxygen affinity constants for biological ammonium and nitrite oxidation, Journal of Chemical Technology & Biotechnology, 80, 388–396, doi:10.1002/jctb.1202, 2005.

Hamme, R. C. and Emerson, S. R.: The solubility of neon, nitrogen and argon in distilled water and seawater, Deep Sea Research Part I: Oceanographic Research Papers, 51, 1517–1528, 2004.

Heiskanen, A.-S. and Leppänen, J.-M.: Estimation of export production in the coastal Baltic Sea: effect of resuspension and microbial decomposition on sedimentation measurements, Hydrobiologia, 316, 211–224, 1995.

HELCOM: Part A. Introductory Chapters, in: Guidelines for the Baltic Monitoring Programme for the Third Stage, no. 27A in Baltic Sea Environment Proceedings, Baltic Marine Environment Protection Commission - Helsinki Commission, Helsinki, 1988.

Hooke, R. and Jeeves, T. A.: "Direct Search"Solution of Numerical and Statistical Problems, Journal of the ACM (JACM), 8, 212–229, 1961.

Ingall, E. and Jahnke, R.: Influence of water-column anoxia on the elemental fractionation of carbon and phosphorus during sediment diagenesis, Marine Geology, 139, 219–229, 1997.

IOW: IOWDB - the oceanographic database of IOW, https://www.io-warnemuende.de/iowdb.html, 2017.

Jaisi, D. P., Dong, H., and Liu, C.: Influence of biogenic Fe (II) on the extent of microbial reduction of Fe (III) in clay minerals nontronite, illite, and chlorite, Geochimica et Cosmochimica Acta, 71, 1145–1158, 2007.

Jakobsen, R. and Postma, D.: Formation and solid solution behavior of Ca-rhodochrosites in marine muds of the Baltic deeps, Geochimica et Cosmochimica Acta, 53, 2639–2648, doi:10.1016/0016-7037(89)90135-X, 1989.

Jonsson, P., Carman, R., and Wulff, F.: Laminated sediments in the Baltic: a tool for evaluating nutrient mass balances, Ambio, pp. 152–158, 1990.

Jørgensen, B. B.: Bacteria and Marine Biogeochemistry, in: Marine Geochemistry, edited by Schulz, H. D. and Zabel, M., pp. 169–206, Springer-Verlag, Berlin/Heidelberg, dOI: 10.1007/3-540-32144-6_5, 2006.

Kersten, M., Leipe, T., and Tauber, F.: Storm disturbance of sediment contaminants at a Hot-Spot in the Baltic Sea assessed by 234Th radionuclide tracer profiles, Environmental science & technology, 39, 984–990, 2005.

Kowalski, N., Dellwig, O., Beck, M., Grunwald, M., Dürselen, C.-D., Badewien, T. H., Brumsack, H.-J., van Beusekom, J. E., and Böttcher, M. E.: A comparative study of manganese dynamics in the water column and sediments of intertidal systems of the North Sea, Estuarine, Coastal and Shelf Science, 100, 3–17, doi:10.1016/j.ecss.2011.03.011, 2012.

Kristensen, E., Ahmed, S. I., and Devol, A. H.: Aerobic and anaerobic decomposition of organic matter in marine sediment: which is fastest?, Limnology and Oceanography, 40, 1430–1437, 1995.

Kulik, D. A., Kersten, M., Heiser, U., and Neumann, T.: Application of Gibbs Energy Minimization to Model Early-Diagenetic Solid-Solution Aqueous-Solution Equilibria Involving Authigenic Rhodochrosites in Anoxic Baltic Sea Sediments, Aquatic Geochemistry, 6, 147–199, 2000.

Large, W. G., McWilliams, J. C., and Doney, S. C.: Oceanic vertical mixing: A review and a model with a nonlocal boundary layer parameterization, Reviews of Geophysics, 32, 363–403, 1994.

Leipe, T., Tauber, F., Vallius, H., Virtasalo, J., Uścinowicz, S., Kowalski, N., Hille, S., Lindgren, S., and Myllyvirta, T.: Particulate organic carbon (POC) in surface sediments of the Baltic Sea, Geo-Mar Lett, 31, 175–188, 2011.

Leppäranta, M. and Myrberg, K.: Physical oceanography of the Baltic Sea, Springer Science & Business Media, 2009.

Lijklema, L.: Interaction of orthophosphate with iron (III) and aluminum hydroxides, Environmental Science & Technology, 14, 537–541, 1980.

Lipka, M.: Current biogeochemical processes and element fluxes in surface sediments of temperate marginal seas (Baltic Sea and Black Sea), Ph.D. thesis, University of Greifswald (Germany), Greifswald, 2018.

Lipka, M. and Böttcher, M. E.: Spatiotemporal dynamics in benthic solute reservoirs of southern Baltic Sea sediments, in prep.

Middelburg, J. J.: A simple rate model for organic matter decomposition in marine sediments, Geochimica et Cosmochimica Acta, 53, 1577–1581, 1989.

Millero, F. J.: Thermodynamics of the carbon dioxide system in the oceans, Geochimica et Cosmochimica Acta, 59, 661–677, doi:10.1016/0016-7037(94)00354-O, 1995.

Millero, F. J. and Leung, W. H.: The thermodynamics of seawater at one atmosphere, American Journal of Science, 276, 1035–1077, doi:10.2475/ajs.276.9.1035, 1976.

Millero, F. J., Sotolongo, S., and Izaguirre, M.: The oxidation kinetics of Fe(II) in seawater, Geochimica et Cosmochimica Acta, 51, 793–801, doi:10.1016/0016-7037(87)90093-7, 1987.

Morse, J. W., Millero, F. J., Cornwell, J. C., and Rickard, D.: The chemistry of the hydrogen sulfide and iron sulfide systems in natural waters, Earth-Science Reviews, 24, 1–42, doi:10.1016/0012-8252(87)90046-8, 1987.

Morys, C.: Particle dynamics in sediments of the western Baltic Sea, Ph.D. thesis, University of Rostock (Germany), Rostock, http://rosdok.uni-rostock.de/file/rosdok_disshab_0000001661/rosdok_derivate_0000035932/Dissertation_Morys_2017.pdf, 2016.

Morys, C.: Seasonality of bioturbation - what governs the intensity of local and non-local sediment mixing?, in prep.

Morys, C., Forster, S., and Graf, G.: Variability of bioturbation in various sediment types and on different spatial scales in the southwestern Baltic Sea, Marine Ecology Progress Series, 557, 31–49, doi:10.3354/meps11837, 2016.

Morys, C., Powilleit, M., and Forster, S.: Bioturbation in relation to the depth distribution of macrozoobenthos in the southwestern Baltic Sea, Marine Ecology Progress Series, 579, 19–36, doi:10.3354/meps12236, 2017.

Neumann, T.: Towards a 3D-ecosystem model of the Baltic Sea, Journal of Marine Systems, 25, 405–419, doi:10.1016/S0924-7963(00)00030-0, 2000.

Neumann, T., Siegel, H., and Gerth, M.: A new radiation model for Baltic Sea ecosystem modelling, Journal of Marine Systems, 152, 83–91, doi:10.1016/j.jmarsys.2015.08.001, 2015.

Oliveros-Ramos, R. and Shin, Y.-J.: Calibrar: an R package for fitting complex ecological models, arXiv preprint arXiv:1603.03141, 2016.

Paraska, D. W., Hipsey, M. R., and Salmon, S. U.: Sediment diagenesis models: Review of approaches, challenges and opportunities, Environmental Modelling & Software, 61, 297–325, doi:10.1016/j.envsoft.2014.05.011, 2014.

Raaphorst, W. V. and Malschaert, J. F. P.: Ammonium adsorption in superficial North Sea sediments, Continental Shelf Research, 16, 1415–1435, doi:10.1016/0278-4343(95)00081-X, 1996.

Radtke, H. and Burchard, H.: A positive and multi-element conserving time stepping scheme for biogeochemical processes in marine ecosystem models, Ocean Modelling, 85, 32–41, 2015.

Radtke, H., Neumann, T., Voss, M., and Fennel, W.: Modeling pathways of riverine nitrogen and phosphorus in the Baltic Sea, Journal of Geophysical Research, 117, C09 024, doi:10.1029/2012JC008119, 2012.

Reed, D. C., Slomp, C. P., and Gustafssonb, B. G.: Sedimentary phosphorus dynamics and the evolution of bottom-water hypoxia: A coupled benthic–pelagic model of a coastal system, Limnol. Oceanogr, 56, 1075–1092, 2011.

Rickard, D. and Luther, G. W.: Kinetics of pyrite formation by the H 2 S oxidation of iron (II) monosulfide in aqueous solutions between 25 and 125 C: The mechanism, Geochimica et Cosmochimica Acta, 61, 135–147, 1997.

Rickard, D. and Luther, G. W.: Chemistry of Iron Sulfides, Chemical Reviews, 107, 514–562, doi:10.1021/cr0503658, 2007.

Rusch, A., Forster, S., and Huettel, M.: Bacteria, diatoms and detritus in an intertidal sandflat subject to advective transport across the water-sediment interface, Biogeochemistry, 55, 1–27, 2001.

Sarazin, G., Michard, G., and Prevot, F.: A rapid and accurate spectroscopic method for alkalinity measurements in sea water samples, Water Research, 33, 290–294, 1999.

Schippers, A. and Jørgensen, B. B.: Biogeochemistry of pyrite and iron sulfide oxidation in marine sediments, Geochimica et Cosmochimica Acta, 66, 85–92, 2002.

Soetaert, K., Herman, P. M., and Middelburg, J. J.: A model of early diagenetic processes from the shelf to abyssal depths, Geochimica et Cosmochimica Acta, 60, 1019–1040, 1996a.

Soetaert, K., Herman, P. M., Middelburg, J. J., Heip, C., deStigter, H. S., van Weering, T. C., Epping, E., and Helder, W.: Modeling 210Pb-derived mixing activity in ocean margin sediments: diffusive versus nonlocal mixing, Journal of Marine Research, 54, 1207–1227, 1996b.

Soetaert, K., Herman, P. M., Middelburg, J. J., Heip, C., Smith, C. L., Tett, P., and Wild-Allen, K.: Numerical modelling of the shelf break ecosystem: reproducing benthic and pelagic measurements, Deep Sea Research Part II: Topical Studies in Oceanography, 48, 3141–3177, 2001.

Stephenson, M. and Stickland, L. H.: Hydrogenase: The reduction of sulphate to sulphide by molecular hydrogen, Biochemical Journal, 25, 215, 1931.

Struck, U., Pollehne, F., Bauerfeind, E., and v. Bodungen, B.: Sources of nitrogen for the vertical particle flux in the Gotland Sea (Baltic Proper)—results from sediment trap studies, Journal of Marine Systems, 45, 91–101, doi:10.1016/j.jmarsys.2003.11.012, 2004.

Stumm, W. and Morgan, J. J.: Aquatic chemistry: chemical equilibria and rates in natural waters, vol. 126, John Wiley & Sons, 2012.

Sun, M., Aller, R. C., and Lee, C.: Early diagenesis of chlorophyll-a in Long Island Sound sediments: A measure of carbon flux and particle reworking, Journal of Marine Research, 49, 379–401, 1991.

Sundby, B., Gobeil, C., Silverberg, N., and Mucci, A.: The phosphorus cycle in coastal marine sediments, Limnol. Oceanogr, 37, 1992.

Tauber, F.: Online-Karte: Sedimentverteilung auf dem Meeresboden, https://www.geoseaportal.de/mapapps/resources/apps/sedimentverteilung_auf_dem_meeresboden/index.html?lang=de, 2012.

Turekian, K. K.: Oceans, Prentice-Hall, 1968.

Uppala, S. M., Kållberg, P. W., Simmons, A. J., Andrae, U., Bechtold, V. d., Fiorino, M., Gibson, J. K., Haseler, J., Hernandez, A., and Kelly, G. A.: The ERA-40 re-analysis, Quarterly Journal of the royal meteorological society, 131, 2961–3012, 2005.

van Cappellen, P. and Wang, Y.: Cycling of iron and manganese in surface sediments; a general theory for the coupled transport and reaction of carbon, oxygen, nitrogen, sulfur, iron, and manganese, American Journal of Science, 296, 197–243, doi:10.2475/ajs.296.3.197, 1996.

van de Bund, W. J., Ólafsson, E., Modig, H., and Elmgren, R.: Effects of the coexisting Baltic amphipods Monoporeia affinis and Pontoporeia femorata on the fate of a simulated spring diatom bloom, Marine Ecology Progress Series, 212, 107–115, 2001.

Voss, M. and Struck, U.: Stable nitrogen and carbon isotopes as indicator of eutrophication of the Oder river (Baltic Sea), Marine Chemistry, 59, 35–49, 1997.

Wasmund, N.: Occurrence of cyanobacterial blooms in the Baltic Sea in relation to environmental conditions, International Review of Hydrobiology, 82, 169–184, 1997.

Westrich, J. T. and Berner, R. A.: The role of sedimentary organic matter in bacterial sulfate reduction: the G model tested, Limnology and oceanography, 29, 236–249, 1984.

Wijsman, J. W. M., Herman, P. M. J., Middelburg, J. J., and Soetaert, K.: A Model for Early Diagenetic Processes in Sediments of the Continental Shelf of the Black Sea, Estuarine, Coastal and Shelf Science, 54, 403–421, doi:10.1006/ecss.2000.0655, 2002.

Winde, V., Böttcher, M., Escher, P., Böning, P., Beck, M., Liebezeit, G., and Schneider, B.: Tidal and spatial variations of DI13C and aquatic chemistry in a temperate tidal basin during winter time, Journal of Marine Systems, 129, 396–404, doi:10.1016/j.jmarsys.2013.08.005, 2014.

Yakushev, E. V., Protsenko, E. A., Bruggeman, J., Wallhead, P., Pakhomova, S. V., Yakubov, S. K., Bellerby, R. G. J., and Couture, R.-M.: Bottom RedOx Model (BROM v.1.1): a coupled benthic–pelagic model for simulation of water and sediment biogeochemistry, Geosci. Model Dev., 10, 453–482, doi:10.5194/gmd-10-453-2017, 2017.